UNIVERSITY OF OKLAHOMA

GRADUATE COLLEGE

# TRANSIENT BRAIN-WIDE NEURONAL ACTIVATIONS IN NONHUMAN PRIMATE UNDER RESTING AND ANESTHETIZED CONDITIONS

A THESIS

SUBMITTED TO THE GRADUATE FACULTY

in partial fulfillment of the requirements for the

Degree of

MASTER OF SCIENCE

By

VALARIE MARIAH IVEY
Norman, Oklahoma
2023

TRANSIENT BRAIN-WIDE NEURONAL ACTIVATIONS IN NONHUMAN PRIMATE UNDER RESTING AND ANESTHETIZED CONDITIONS

A THESIS APPROVED FOR THE

STEPHENSON SCHOOL OF BIOMEDICAL ENGINEERING

BY THE COMMITTEE CONSISTING OF

Dr. Lei Ding, Chair

Dr. Hong Liu

Dr. Rebecca Scott

**Acknowledgements**

I would like to thank Dr. Lei Ding for mentoring, encouraging, and guiding me through this research project and helping me obtain the base knowledge I needed to pursue this thesis.

I would also like to thank my thesis committee members, Dr. Rebecca Scott and Dr. Hong Liu, for sitting on this committee.

I would also like to thank a member of my research team, Thuy L. Nguyen, in Dr. Lei Ding's Neuroimaging and Neural Engineering Lab for helping me process a portion of the data in this research, as well as Dr. Shou Guofa for providing me guidance in processing and analysis of the acquired data in this research.

# Table of Contents

Acknowledgements…… iv

List of Tables……... viii

List of Figures…… ix

Abstract……... x

Chapter 1: Overview and Scope of Research……. 1

1.1 Significance…….. 1

1.2 Existence of Brain-wide Patterns……. 3

1.3 Objectives and Findings……... 4

1.4 Organization of Thesis...…….. 5

Chapter 2: Background……... 6

2.1 fMRI…….. 6

2.2 EEG……... 6

2.3 ECoG……. 8

2.4 Rationale Behind Study.……..……..……...… 9

Chapter 3: Experimental Materials and Methods……. 12

3.1 Monkey Data Acquisition and Processing…….. 12

3.2 Human Data Acquisition and Processing…… 15

3.2.1 EEG Processing……... 15

3.2.2 Cortical Source Imaging…….. 15

3.3 CAP Analysis via Clustering……... 17

3.4 Spatial and Temporal Metrics for Evaluating Similarities/Differences Between Human and Monkey CAPs……. 18

3.5 Derivation of Optimal K-value……...…… 20

Chapter 4: Identification of Transient Brain-wide CAPS in Monkeys…….…… 22

4.1 Spatial Patterns in Monkey ECoG Data……...… 22

4.2 Temporal Patterns in Monkey ECoG Data…….…… 27

4.3 Transitional Patterns in Monkey ECoG Data……...… 30

Chapter 5: Comparison to Identified Transient Brain-wide CAPs in Human……..…… 34

5.1 Spatial Patterns……...……...……. 34

5.2 Temporal Patterns……..……. 38

5.3 Transitional Patters…….…… 40

5.4 Summary of Similarities Between Monkeys and Humans…….…… 43

Chapter 6: Comparison of Phenomena Between Anesthesia and Resting Monkey ECoG Data……... 45

6.1 Spatial Patterns in Anesthesia Monkey Data…….. 45

6.2 Temporal Patterns in Anesthesia Monkey Data……...… 48

6.3 Key Observed Similarities/Differences……..…… 51

Chapter 7: Discussion……..……. 53

7.1 Discoveries and Comparison to Literature……..…… 53

7.2 Conclusion……..…… 54

7.3 Summary……..… 55

7.4 Limitations and Future Studies……..……. 57

References…….…… 59

# List of Tables

Table 1: Available Monkey ECoG Sessions with Resting Conditions……..… 14

Table 2: Summary of Significant Similarities between Monkey and Human Data…….. 45

# List of Figures

Figure 3.1 Explained variance as a function of cluster number……..…..…… 21

Figure 4.1 Spatial patterns on Monkey S……..… 23

Figure 4.2 CAPs for the left hemisphere in all four monkeys…….……. 26

Figure 4.3 Temporal metrics of the four monkeys……...……. 29

Figure 4.4 Occurrence transitional patterns of the four monkeys…...…….. 32

Figure 4.5 Lifetime transitional patterns of the four monkeys……...…….. 33

Figure 5.1 Human and monkey CAPs for both hemispheres……..……...…..……. 37

Figure 5.2 Temporal metrics of humans……..……...…….. 39

Figure 5.3 Occurrence and lifetime transitional patterns of humans and Monkey S…… 41

Figure 6.1 Spatial patterns of anesthetized monkeys……..... 47

Figure 6.2 Temporal patterns of anesthetized monkeys…… 50

Figure 6.3 Transitional patterns of anesthetized monkeys…… 52

# Abstract

The aim of this thesis was to determine the existence of and identify transient brain-wide patterns in nonhuman primates if these patterns did exist. Specifically, this thesis revolves around identification of coactivation patterns (CAPs). Through observation of these CAPs derived from timeframe-wise cluster analysis, other questions arose: do these patterns I identified in monkeys show some correspondence to those in a different species using different modalities of neuroimaging, focusing on humans in the present thesis, and how do these patterns present in varying levels of consciousness within the same species using the same imaging technique?

Using electrocorticography (ECoG) monkey data, I have identified the existence of CAPs in monkeys as well as observed spatiotemporal patterns these activations exhibited in the resting state, the characteristics of neural networks which are similar to humans. Using human electroencephalography (EEG) data, I have also compared the results of monkey ECoG resting data analysis against human CAPs and found significant similarities in spatial, transitional, and temporal patterns between the two species.

Finally, I compared the same results from the monkey ECoG resting data analysis to patterns found in anesthetized conditions of nonhuman primates and found differences in the spatial and temporal characteristics of brain-wide coactivations between these different states of consciousness within the same species.

# Chapter 1

## Overview and Scope of Research

### 1.1 Summary and Significance

Many studies have been conducted using electroencephalography (EEG) and magnetoencephalography (MEG) to validate the existence of brain-wide patterns found previously in other studies utilizing fMRI (Brookes et al., 2011, Yuan et al., 2016). In fact, due to the high temporal resolution of EEG (milliseconds), such studies obtained encouraging results that only complemented findings from fMRI. These included the observation of fast dynamics displayed in brain-wide patterns (Baker et al., 2014, Ding et al., 2022) as well as frequency-specific patterns (Becker and Hervais-Adelman, 2020, Vidaurre et al., 2018), and they allowed us to observe brain-wide patterns from a primary response (electrical) beyond those stemming from observation of the secondary hemodynamic-based response provided by fMRI.

Furthermore, animal neuronal data obtained from noninvasive imaging have also provided more insight into brain-wide pattens across species (Matsui et al., 2016), possibly providing us with a means of using animal models to further research into behaviors exhibited from fast dynamics and frequency-specific patterns brain-wide phenomena. This possibility allows us to manipulate these brain-wide phenomena using a means not possible with human studies, e.g., via invasive manipulations and measurements of neural activity, and pharmaceutical manipulations.

Being able to find neural network characteristics across species (human and monkey) that are congruous between them will only support the idea of transient patterns

being reserved through evolution, implying there is a potential link in the neural responses and behavior between humans and monkeys when they receive the same stimulus or exposed to the same conditions. This link is one needed to be able to further support the use of an animal model to perform more invasive studies.

In this thesis I investigated the possible presence of a set of fast coactivation patterns (CAPs) (with the lifetime around 100 milli-seconds), representing brain-wide transient neuronal events that have been identified recently from human EEG data (Ding et al., 2022), in non-primate animals. To test this hypothesis, I used electrocorticography (ECoG) data of four macaque monkeys, available from the public domain, neurotycho.org, with the whole high-density electrode coverage of either one hemisphere or two hemispheres and high-density EEG data from 34 human subjects recorded in Dr. Lei Ding's Neuroimaging and Neural Engineering lab. To identify the CAPs in both monkey ECoG data and human EEG data, I performed a timeframe-wise clustering analysis directly on time-course data from ECoG electrodes and inversely mapped and cortical-parcel-averaged current source time-course data from EEG using the procedure reported in a previous study (Shou et al., 2022). The results indicated that a set of alpha band frequency-specific fast CAPs (with the mean lifetime of ~100 milli-seconds) could be identified in monkey ECoG data, which shared the similar spatial, temporal, and transitional properties in the set of CAPs identified from human EEG data. These results provide the first set of evidence, suggesting that frequency-specific fast brain-wide phenomena are also reserved across species beyond those slow ones from blood-oxygen-level-dependent (BOLD) functional magnetic resonance imaging (fMRI).

This thesis will expound on brain-wide coactivation patterns found in animals, i.e., monkeys, and their relationship to those found in humans as well as different states of consciousness within the same species (nonhuman primate), supporting results in previously mentioned animal species, only with a more invasive means. The use of ECoG data provides me with clearer activity levels and their locations due to the direct contact of electrodes with the surface of the brain.

### 1.2 Existence of brain-wide patterns

The brain has many states in which self-organized continuously changing dynamics of neural networks define them, which also involve interaction between different regions of the brain (Kringelbach and Deco, 2020). These are important to understanding behavior and function of the brain during different brain states and how neural network structure relates to neural responses and biological function. Understanding these connections is vital to progressing in scientific studies encompassing neurological and physiological diseases, such as epilepsy. Early studies involving observation of such activities were able to discover functionally correlated regions of the brain were activating synchronously at rest and showed to be highly spatiotemporally organized throughout the brain, forming what is now known as the so-called resting-state network (RSN) (van den Heuvel et al., 2009, Liu et al., 2013).

Building off the identification of RSNs, many other brain-wide spatiotemporal patterns have emerged throughout many studies that offer direct insight as to the potential drivers behind the formation of the RSN. These include but are not limited to quasiperiodic patterns (QPPs), global propagating waves (GPWs), and CAPs (Liu et al., 2013, Ding et al., 2022, Abbas et al., 2019, Thompson et al., 2014, Gu et al., 2021, Khan et al., 2022).

These patterns are vital in the understanding of intrinsic neural activity and brain functions (Gu et al., 2021). A recurring existence of RSNs and other brain-wide spatiotemporal patterns have also been observed across species, i.e., mice, nonhuman primates (macaque) and humans (Majeed et al., 2011, Sforazzini et al., 2014, Hutchison et al., 2011, Hutchison and Everling, 2012, Gozzi and Schwarz, 2016). Not only have brain-wide patterns been proven to exist across species, but much of these spatiotemporal patterns in animal studies have also shown to be similar to those in human studies (Massimini et al., 2004, Stroh et al., 2013, Matsui et al., 2016, Gu et al., 2021). Finding a direct connection in brain-wide patterns between differing species in different states of consciousness, specifically in a direct comparison to humans, could have a significant impact on further research into a broad spectrum of different research fields, from pharmaceuticals to diseases and diagnosing these diseases (Chen et al., 2019, Shou et al., 2017, Zhu et al., 2013), possibly proving to be vital in both clinical and research settings (Auer, 2008, van den Heuvel and Hulshoff Pol, 2010) along with having limitless potentials within these many settings. To be able to observe many of these brain-wide patterns scientists have implemented the use of many different neuroimaging modalities. These include the use of functional magnetic resonance imaging (fMRI), electroencephalography (EEG), and electrocorticography (ECoG).

### 1.3 Objectives and findings

The first objective of this study is to determine if nonhuman primates have similar neural activations as humans during the resting state. I aim to find the existence of co(de)-activations (CAPs).

The second objective is to observe spatial, temporal, and transitional patterns for the CAPs and briefly determine if there are similar networks that provide the same or similar patterns within these CAPs between nonhuman primates and humans.

The final objective is to observe either similar or differing patterns exhibited in nonhuman primates during different states of consciousness, specifically the resting state and anesthesia conditions.

### 1.4 Organization of Thesis

In chapter 2 I will present the background of functional magnetic resonance imaging (fMRI), electroencephalography (EEG), and electrocorticography (ECoG) in some detail and why I am using such data from specifically EEG and ECoG imaging modalities to observe coactivations. In chapter 3 I will move onto the different methods used to acquire and process resting state EEG data from humans that was provided by another study (Shou et al., 2022) and resting state ECoG data from nonhuman primates provided in an open source (neurotyhco.org) by a research group in Japan (Oosugi et al., 2017). I will also discuss the process used to organize specific activation groups and their temporal patterns. In chapter 4 I will discuss the existence of CAPs found within the monkey ECoG data. In chapter 5 I will talk about the spatial, temporal, and transitional patterns found in the monkey ECoG data and establish whether these same patterns were observed in human data as well. In chapter 6 I will transition to the patterns found in monkey anesthesia data and how these patterns compare to monkey data in the resting state, which were discussed in chapter 4. Finally, I will present the discussion, future studies, and summary in chapter 7.

# Chapter 2

# Background

## 2.1 Functional Magnetic Resonance Imaging (fMRI)

Functional magnetic resonance imaging (fMRI) has made its way to the forefront in observing brain activity. It monitors the behavior and characteristics of blood and how these change during different stimuli by using the connection of how electrical activity interacts with physiology during different conditions (hemodynamic responses) to explore neural (de)activations. Specifically, it is used to observe fluctuations in what is known as the blood-oxygen-level-dependent (BOLD) signal to determine the functional architecture of the brain, as it is sensitive to the changes in oxygenation of hemoglobin (Lee et al., 2013, Ogawa et al., 1990). In other words, this method to monitor neural activity is through measurement of a secondary response, not the primary response, and offers little indication of the origin of neuronal signals. Although it offers a high spatial resolution compared to other neuroimaging methods, it has low temporal resolution. This imaging technique has been utilized and proven valuable in clinical settings to study disease states, such as Alzheimer disease, and for presurgical planning of procedures such as those for finding seizure foci in epileptic patients (Lee et al., 2013).

## 2.2 Electroencephalography (EEG)

Neurons are electrically excitable cells responsible for processing and transmitting information via synapses by using electrical and chemical signals for communication. Electroencephalography (EEG) is a noninvasive imaging method that uses electrodes to sense and measure the induced magnetic fields from the current created by these neurons

(Hamalainen and Ilmoniemi, 1994). Initial signals from this noninvasive method of a human brain were recorded by Hans Berger, a German physiologist in 1924 (Haas, 2003). The magnetic fields induced by neuronal current are very weak, however, approximately one billionth of that of earth's, emphasizing the need for detectors sensitive enough to sense these electrophysiological signals (Baillet, 2001, Hamalainen and Ilmoniemi, 1994) . Since 1924, many decades of research and development have led to more efficient designs of electrodes and their layout. A 10/20 system is now used to which the location and names of the electrodes were standardized by the American Electroencephalography Society (Malmivuo et al., 1995, Sharbrough, 1991). EEG involves electrodes fixed on a cap or net being placed on the scalp (He, 2020) and is incapable of detecting individual and direct signals; it detects the net outcome of tiny magnitudes of signals that are integrated from thousands to millions of neurons (Wendel et al., 2008, van den Broek et al., 1998), making this method of imaging one with low spatial resolution, but it has a high temporal resolution in order of milliseconds. The signals detected do not have a direct correspondence to their location in the brain either, so to localize the source of the signal other imaging methods are used in conjunction with EEG, such as MRI (Magnetic Resonance Imaging), to use as a map of the brain in which a biophysics model can be developed to generalize the location. Over the span of the decades following the initial recording of EEG signals from a human brain, imaging has evolved to trace these signals to their cortical origin and map them in their corresponding locations (Hamalainen and Ilmoniemi, 1994, Matsuura and Okabe, 1995, Uutela et al., 1999, Darvas et al., 2004, Ding, 2009b, Ding, 2012, Ding and He, 2008, Ding et al., 2005, Zhu et al., 2014). The neuronal signals detected by EEG also must travel through many layers, such as hair, scalp, and cerebral spinal fluid (CSF), which causes a

high impedance that attenuates the signals, leading to smeared EEG measurements. This is known as the volume conduction effect (Cohen and Cuffin, 1983, Lai et al., 2005). Applying a liquid or a gel conductive electrolyte directly to the electrodes used in EEG can reduce the impedances that contribute to the volume conduction effect (Malmivuo et al., 1995).

### 2.3 Electrocorticography (ECoG)

Electrocorticography (ECoG) is an invasive modality for measuring electrical potentials derived from neuronal signals in various cortical areas (Rubehn et al., 2009, Viventi et al., 2011). Electrodes are placed directly on the cortical surface of the brain and require an expensive clinical surgery for subdural placement of the electrode array (Khodagholy et al., 2016, Asano et al., 2009, Kuruvilla and Flink, 2003, Zhang, 2006). This method is typically used in nonhuman animal studies due to the risk of complications involved in exposing the brain and invasiveness. It is utilized to record data that could be used for diagnosis, expound on areas involving mapping cortical functions, and investigating functional mechanisms of brain oscillations (Potes et al., 2012, Gunduz et al., 2012, Mesgarani and Chang, 2012, Crone et al., 1998, Daitch et al., 2013, Watrous et al., 2015, Lai, 2019, Lai, 2020). ECoG was developed in the 1940s and was initially used as a diagnostic procedure to locate seizure foci in a conscious human epileptic patient (Ding, 2009a), usually preceded by EEG to obtain an initial general location of the onset zones (Viventi et al., 2011, Geddes, 1996, Branco et al., 2023). It offers a higher spatial resolution than EEG that can detect in the order of millimeters and has a temporal resolution similar to EEG in the millisecond range (Todaro et al., 2019, Hill et al., 2012). ECoG also has a higher signal to noise ratio (SNR) than EEG due to the electrodes being placed directly on

the surface of the brain instead of the scalp and is less susceptible to artifacts (Hill et al., 2012, Yanagawa et al., 2013). Due to having to open the skull to place the electrode array however, there is limited coverage over the brain. Nonhuman primates can offer a larger surface coverage of the cortex (Yanagawa et al., 2013, Takaura et al., 2016). The electrodes used for ECoG are imbedded in silicon sheets and detect signal amplitudes that are five times higher than those obtained from scalp recordings (Branco et al., 2023, Blume and Holloway, 2011). The layout of electrodes is usually in an NxM array or strips of 1xN electrodes with inter-electrode distance of up to 10mm and an exposed electrode surface diameter of 2.5mm (Branco et al., 2023, De Salles et al., 1994, Diehl and Luders, 2000, Lesser et al., 2010, Penfield and Boldrey, 1937).

### 2.4 Rationale Behind Study

The brain is an integrative network in which functionally linked regions can process information to obtain and achieve specialized functions throughout the body (van den Heuvel and Hulshoff Pol, 2010). There have been many advancements in different imaging techniques to monitor these many brain functions along with brain structure. With modalities such as fMRI, magnetoencephalography (MEG), EEG, and ECoG, researchers have been able to explore how neurons interact with each other, the networks they form and their dynamics, and the correspondence of behavior to distinct regions of the brain (Arfanakis et al., 2000, Fox and Raichle, 2007, Fox et al., 2006, Hampson et al., 2002). Using this reenforced background in neuroscience scientists have been able to delve deeper into observing many different patterns the brain exhibits during dissimilar stages of consciousness, such as resting awake (Hampson et al., 2002, Cordes et al., 2000, Greicius et al., 2003), and anesthetized (Liu et al., 2015) states. Among the many techniques to

observe these patterns fMRI has predominated as an indirect measure of neural activations and their origins. In fact, studies using analysis of human fMRI data have determined the existence of brain-wide phenomena called global propagating wave (GPWs) (Raut et al., 2021), and quasiperiodic patterns (QPPs) (Abbas et al., 2019, Thompson et al., 2014). However, due to the indirect nature of measuring blood-oxygen-level-dependent (BOLD) signals as an indicator for neural activity, having low temporal resolution from the time is takes the secondary activation to occur and being unable to record fast activations, scientists have been actively investigating neural activations and their origins utilizing other means for obtaining this information directly. Among these many methods to measure and analyze neural signals with characterizations similar to RSNs generated from primary neural response processes, EEG (Custo et al., 2017, Ding et al., 2022, Yuan et al., 2016) and ECoG (Betzel et al., 2019) have offered further insight into localizing source signals neurons emit in specific regions of the brain and their formation of networks during different states of consciousness as well as the existence of brain-wide patterns, such as transient coactivation patterns (CAPs) (Liu and Duyn, 2013). EEG is noninvasive, inexpensive, and has a high temporal resolution, making it ideal to use to record neural activity in the human brain. ECoG on the other hand is very invasive, requiring surgery to expose the surface of the brain to place electrodes in direct contact with the cortical surface. This method is usually reserved for animal studies and humans with epilepsy for their diagnosis and treatment of the disease. Using techniques such as these, scientists have been able to prove there is functional connectivity between regions of the human brain and spontaneous neural activity within these regions during times of rest that activate synchronously for brain functions, forming the resting state network (RSN) (Cordes et al.,

2000, Hampson et al., 2002, Greicius et al., 2003, Liu et al., 2013, van den Heuvel et al., 2009). Both imaging methods can directly measure primary neural activity and fast activations with higher temporal resolutions than fMRI (Shou et al., 2020). Brain-wide patterns help in observing how the brain forms networks in different conditions and the dynamics between different regions in which these network connections are formed, which are made apparent in from the study of CAPs. Analyzing CAPs involves using cluster-based analysis, unlike correlation calculations used primarily in the past with EEG data to find correspondence between regions of the brain in which there is an inability to see the fast dynamic responses that are observed in CAPs. This inability to observe fast dynamic responses is due to the fact that correlation calculations are performed during predetermined intervals of time, whereas CAP analysis involves comparison of different regions of the brain over a continuous period of time. With ECoG and EEG imaging techniques, fast brain-wide neural CAPs can be analyzed to observe the primary neural activity through the use of clustering to observe them and their spatial, temporal, and transitional characteristics.

# Chapter 3

## Experimental Materials and Methods

### 3.1 Monkey Data Acquisition and Processing

Electrocorticography (ECoG) data of 4 macaque monkeys (Monkeys C, G, K, and S) was obtained from a public shared source (neurotycho.org). Detailed methods and protocols of experimental, surgical, and recording procedures can be found in literatures (Nagasaka et al., 2011, Yanagawa et al., 2013). All studies were approved by the RIKEN ethics committee and in accordance with the recommendations of the Weatherall report, "The use of non-human primates in research".

Briefly, a customized 128-channel electrode array (Unique Medical, Japan) was implanted into the subdural space of the left hemisphere of each monkey, except for Monkey S having one experiment of 256 channels available with a 128-channel electrode array on both the left and right hemisphere of the brain. Array coverage was contiguous over the parietal, temporal, occipital, and frontal lobes with electrode spacing at 5 mm. There was also middle wall coverage on Monkey C and Monkey G. The electrodes were 3 mm in diameter and consisted of platinum discs. Reference electrodes were implanted in the subdural space and ground electrodes in the epidural space. A total of 32 experiments were conducted over different days and monkeys. Each experiment included the eyes-closed waking condition and 1 of the following 3 conditions: ketamine/medetomidine anesthesia, propofol anesthesia, or natural sleep except for the resting experiment for Monkey C and Monkey S consisting solely of the eyes-closed waking condition. The monkey was sitting calmly, and the ECoG signals were recorded for up to 20 min during

this eyes-closed condition before the administration of anesthesia drugs or natural sleep. For the experiments of anesthesia, the loss of consciousness (LOC) was defined behaviorally (see details in Nagasaka et al., 2011) and after that, neural activity, which is characterized by slow-wave activity, was recorded for ~25 min with heart rate and breathing monitored carefully. For the experiments that included the natural sleep condition, electro-oculography (EOG) and electromyography (EMG) signals were monitored and used together with ECoG to determine the onset of sleep (see details in Nagasaka et al., 2011). All ECoG and other electrical recordings, i.e., EMG and EOC, were sampled at 1 kHz by the Cerebus data acquisition system (Blackrock, UT, USA).

There were 32 recordings (Table 1) from four monkeys. In the present study, we focused our analysis on ECoG data from awake conditions and, therefore, resting data (awake with eyes covered) before the administration of anesthesia drugs or natural sleep were extracted firstly according to the experimental protocol described above. The extracted recordings for resting awake conditions ranged in length from 5 to 20 minutes, which were then independently preprocessed using EEGLAB (Delorme and Makeig, 2004). Each extracted dataset was filtered using a notch filter with the band-stop frequency at 50 Hz to remove powerline noises. Zero to four bad channels were identified and removed in each dataset and then data in these channels were interpolated with data from their surrounding channels. Each dataset was then bandpass-filtered at 0.5 Hz-150 Hz then re-referenced using the common average reference. It is noted that no ECoG segments were rejected to maintain the continuity of data.

**Table 1. Available Monkey ECoG Sessions with Resting Conditions**
This is a table of the sessions available for each monkey consisting of resting conditions in their experiment. The number of recordings, length of the recordings with their mean and standard deviation, and the number of electrodes (128/256) used for each recording are given. Note Monkey S has left hemisphere coverage for most recordings and one both hemisphere coverage recording.

| Monkey ID | # of Recordings | Length of Recordings (mins)(mean±std) | Electrode Coverage | # of ECoG Electrodes |
|---|---|---|---|---|
| S | 3 | 20.8 ± 1.1 | Left hemisphere | 128 |
| | 1 | 5.0 ± 0.0 | Both hemispheres | 256 |
| C | 13 | 11.9 ± 5.3 | Left hemisphere | 128 |
| G | 12 | 12.3 ± 4.0 | Left hemisphere | 128 |
| K | 3 | 12.2 ± 0.1 | Left hemisphere | 128 |

### 3.2 Human Data Acquisition and Processing

The human EEG data used in the present analysis was acquired in a previous reported study (see details in Shou et al., 2022). Briefly, resting-state high-density EEG data was obtained from 34 healthy participants (age: 24±5 years, range 18-38 years, 9 females) with informed consents. The study was approved by the Institutional Review Board at the University of Oklahoma Health Science Center (OUHSC). Each dataset had a duration of 10 minutes and was sampled at 1 kHz using a 128-channel Amps 300 amplifier (Electrical Geodesics Inc., OR, USA). Structural MRI was gathered from each participant as well using a GE MR750 scanner with GE's "BRAVO" sequence: FO=240 mm, axial slices per slab=180, slice thickness=1 mm, image matrix=256×256, TR/TE=8.45/3.24 ms.

#### 3.2.1 EEG Processing

All datasets were preprocessed using the exact same procedure on each dataset from each individual participant with EEGLAB (Delorme and Makeig, 2004). Each individual dataset was filtered by a band-pass filter of 0.5–100 Hz, and a notch filter of 58–62 Hz. Noisy channels and independent components (ICs) of artifacts related to ocular, muscular and cardiac activities, were identified by the FASTER plugin (Delorme and Makeig, 2004) with the support of manual visual inspections as well. These artifactual ICs were then removed and data on the identified noisy channels were interpolated with data from their surrounding channels. Finally, each dataset was downsampled to 250 Hz and re-referenced to the common average. It is noted that no EEG segments were rejected to maintain the continuity of data.

#### 3.2.2 Cortical Source Imaging

To map human EEG signals to the similar recording space (i.e., epicortical surface) and spatial resolution as monkey ECoG data, cortical source imaging (Ding et al., 2011, Liao et al., 2013, Liao et al., 2012) was performed to reconstruct brain current sources over the cortical surface from scalp EEG, which deconvoluted the effects of volume conductors of the skull and therefore led to improved spatial separations of different EEG current sources. Via registering the cortical surface from each individual participant to the standard template for human cortex, reconstructed cortical current source data from different human individuals could be converted into the same spatial domain to perform the group-level analysis. These mapping steps transformed data into the unified space (i.e., the cortex) with anatomical definitions of various human brain functional regions, which facilitates the interpretation of obtained CAP results within the human species as well as across the species of human and monkey. In details, individual structural MRI data were segmented using FREESURFER (Fischl, 2012) to extract the surfaces of the scalp, skull, and brain for building individual volume conduction models, and the interface between white and gray matters for the cortical current density (CCD) source model. These surfaces were tessellated into triangular elements (volume conduction model: 10,242 nodes and 20,484 triangles, CCD model: 20,484 nodes and 40,960 triangles). For the CCD model, the nodes on the medial wall adjoining the corpus callosum, basal forebrain, and hippocampus, were excluded from the source space, leading to the total number of sources as 18,715. The electrical conductivities of the scalp, skull, and brain for the volume conduction models were assigned as 0.33/Ωm, 0.0165/Ωm, and 0.33/Ωm, respectively. Electrode locations were registered on the scalp surface by aligning three landmark fiducial points from both EEG and MRI recordings for each individual participant. Based on these models, the

boundary element method (BEM) was used to compute the forward relationship between the scalp EEGs and current source amplitudes of all nodes on individual CCD models. The minimum-norm estimate (Hamalainen and Ilmoniemi, 1994) was then used to reconstruct current source amplitudes of all nodes on individual CCD models from recorded EEG signals at the resolution of individual timeframes, leading to a series of cortical tomography as the function of time at the same temporal resolution of preprocessed EEG data (i.e., 250 Hz, see section 2.2). More details available in (Shou et al., 2022).

### 3.3 CAP Analysis via Clustering

To obtain CAPs from monkey preprocessed ECoG data and human cortical tomographic current source (cTCS) data, a series of processing steps were performed for the preparation of input data to the clustering analysis. Firstly, each dataset from individual recording sessions of individual monkey or individual human participants was filtered into data for different frequency bands, i.e., delta (1-4Hz), theta (5-7Hz), alpha (8-12Hz), beta (13-30Hz), gamma (31-100Hz). This thesis only focused on the alpha-band data. Secondly, instantaneous amplitudes of time courses of alpha-band ECoG data on individual electrodes or alpha-band cTCS data on individual CCD nodes were calculated individually (Baker et al., 2014, Hipp et al., 2012)((Hipp et al., 2012). Thirdly, while the human cTCS data and monkey ECoG data are in the similar spatial domain (cortical surface vs epicortical surface), the spatial dimension of the human cTCS data is much larger than the spatial dimension of the monkey ECoG data (18,715 CCD nodes vs 128/256 ECoG electrodes), which might have an impact on the performance of the clustering analysis. Therefore, a dimension reduction approach was adopted from the previous CAP analysis (Shou et al., 2022). 100 regions of interest (ROIs) were defined over the cortex for each

hemisphere based on an atlas and each ROI represented a parcel of cortical units of functional similarities (Schaefer et al., 2018). ROI-level instantaneous amplitude data were calculated, only for human cTCS instantaneous amplitude data as average values among all cortical sources within the same ROI, which reduced the spatial dimension of human cTCS data to 200 (for the left and right hemispheres together) that are close to the spatial dimension of monkey ECoG data. Fourthly, both ROI-level instantaneous amplitude data for human and electrode-level instantaneous amplitude data for monkey was then converted to z-scores via a within-session normalization (i.e., subtracting the mean and dividing the standard deviation across all time points of each recording session per ROI/electrode). Finally, the K-means clustering was performed using the L1-norm distance as the measure on these normalized datasets with the number of clusters varying from 2 to 20 and the optimal number of clusters for each analysis was selected based on the metric of percentage of explained variance being larger than 90% (Schaefer et al., 2018). In particular, the K-means clustering analysis was performed at the group level in human, in which human ROI-level instantaneous amplitude z-score from the data were concatenated across individual human participants. On the contrary, to evaluate the reproducibility of CAPs from different recording session data of the same monkey, the K-means clustering analysis was performed at the level of individual sessions for each monkey and statistics for quantitative measures of CAPs (see next section, 3.4) were calculated separately for different monkeys. This was designed because the ECoG electrode coverage and positions were different in different monkeys due to not being able to generate group-level statistics of CAPs across monkeys.

### 3.4 Spatial and Temporal Metrics for Evaluating Similarities/Differences Between Human and Monkey CAPs

The outputs of the clustering analysis labeled each timeframe from either human or monkey to one of identified CAPs. The brain-wide spatial tomography of each CAP was defined as the averaged map across all timeframes (z scores) belonging to the CAP, separately for individual recording sessions in monkeys and altogether for data from all human participants (the group level). Multiple temporal metrics calculated for individual CAPs for individual recording sessions based on the clustering labels included *occurrence*, *lifetime, fractional occupancy rate*, and *immediate transition.* It was noted that there were multiple recording sessions per monkey but only one recording session per human participant and, therefore, calculated temporal metric values could also be considered as samples per participant in human. An occurrence of a CAP was defined as multiple consecutive timeframes that were labeled toward the same CAP, and the occurrence rate of a CAP was the ratio between the total number of occurrences of a specific CAP and the total number of occurrences of all CAPs in each recording session. Lifetime of a CAP was defined as the number of consecutive timeframes in an occurrence of the CAP, and its mean lifetime was first calculated in individual recording sessions, and then averaged over all sessions for individual monkeys or all human participants. The fractional occupancy was defined as the total number of timeframes belonging to a CAP divided by the total number of timeframes in each recording session. Immediate transition among CAPs were defined as the transition from one CAP occurrence to the following occurrence of a different CAP. The immediate transition rate of a CAP (at time $t$) to other CAPs (at time $t+1$) is defined as the numbers of transitions from the CAP to other CAPs, divided by the total number of occurrences of the CAP. These session-level measures were then statistically compared between different CAPs or different categories of CAPs using paired t-tests in individual

monkeys. In humans, participant-level measures were similarly statistically compared between different CAPs or varying categories of CAPs.

### 3.5 Derivation of Optimal K-values

Separate cluster analysis on individual session from each monkey, thresholded at 90% of the explained variance, consistently showed the optimal number of CAPs (k-value) for all datasets, ranging between 12 and 13 (Fig. 3.1C), with each output of cluster analysis labeling each time-frame data to one CAP. These k-values also indicated small variations (Fig. 3.1B), supported by small variations of explained variances at differing k-values for each monkey (green shaded area Fig. 3). Using different k-values other than the optimal revealed CAPs having similar patterns to those with the optimal k-value and the similarities grew the closer the k-values got to the optimal k-value. Human k-value was lower than the average monkey k-value at 8 (Fig. 3A). The exponential curves in Figure 3.1A and 3.1C are all similar in that they all have an increasing pattern, but the rate in which the human data changes is faster than those shown in the monkey data. Another difference between the monkey and human plots is that a higher percentage of variances are explained at a lower number of clusters than for the monkey data (70% in human, 55% in monkey, k-value = 2). It is important to note that k-values other than the optimal one has similar patterns to the optimal, and the patterns become more similar the closer they get to the optimal k-value.

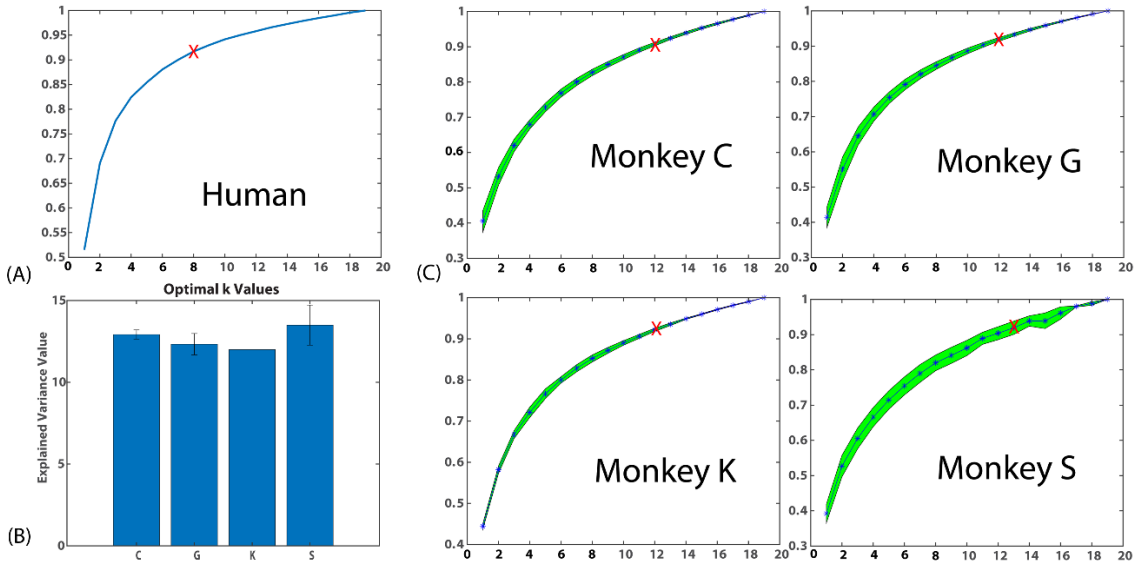


**Figure 3.1**. Explained variance as a function of cluster number. (A) Human k-value determination. In this plot 90% of the explained variance occurred at a cluster number of 8 from 20 clusters, indicated by a red 'x' on the plot. It was derived from group analysis of 34 participants. (B) Average optimal k-value for monkeys. In this bar plot the average k-values for all four monkeys are shown along with their standard errors. They were determined by taking the average k-value across all datasets for each monkey in which the cluster accounted for 90% of the explained variance. (C) Optimal k-values for monkeys. In these plots a total of 20 clusters were analyzed to determine the optimal k-value for each monkey. 90% of the explained variance occurred at cluster 13 for Monkeys C and S, and 12 for Monkeys G and K, shown as a red 'x' on the curve along with the variance for each cluster, displayed in the green shaded region for all plots.

# Chapter 4

## Identification of Transient Brain-wide CAPs in Monkeys

Using the optimal k-value to determine the optimal number of CAPs to observe for each monkey and human, as well as the methods outlined throughout this chapter, I was able to clearly visualize the spatial patterns of these CAPs in monkeys and observe their temporal and transitional characteristics (Chapter 4), then compare these finding to human CAPs (Chapter 5). The same procedure used throughout this chapter was also used to later explore the differences between the resting state and anesthetized state found in monkey ECoG data (Chapter 6).

### 4.1 Spatial Patterns in Monkey ECoG Data

To observe spatial patterns within the monkey ECoG data independent clustering analyses on left-hemisphere ECoG data only and right-hemisphere ECoG data were performed using the data from the both-hemisphere ECoG recording session in Monkey S (seen Fig. 4.1). The results indicated similar spatial patterns of CAPs identified using the left-hemisphere only data, right-hemisphere only data, or both-hemisphere data (Fig. 4.1). Furthermore, the grouping of CAPs with symmetric spatial patterns from the left-hemisphere only data and the right-hemisphere only data seems to have reproduced most CAPs identified from the both-hemisphere data. Based on these observations, I assumed that the CAPs identified from single-hemisphere only data in all four monkeys are representative to CAPs that would be identified if both-hemisphere recording data were available.

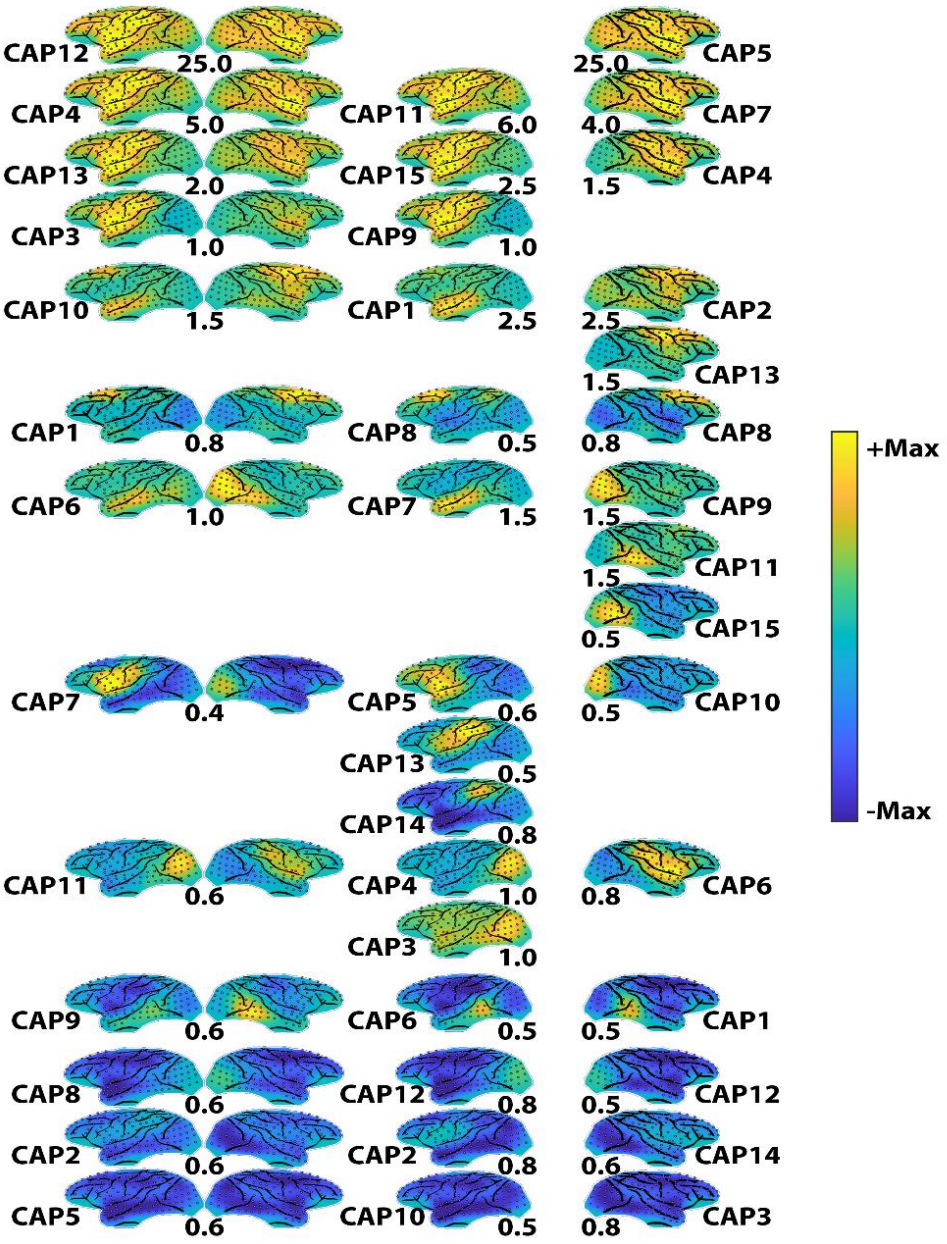


**Figure 4.1.** Spatial patterns on Monkey S. In the resting state, spatial maps of the CAPs of both hemispheres are on the left in two columns. Next is the left hemisphere in the middle column, and finally the right hemisphere in the right most column. The activation amplitudes are provided under each CAP as well as a reference colorbar on the far right. The CAPs are grouped according to activation locations as well as activation intensity for both hemispheres, left hemisphere, and right hemisphere through visual observation. Matching patterns are present of the left and right hemisphere and both hemispheres even with separate processing of the three groups. The CAPs are also organized in descending order activation amplitudes starting with the GHA group, then the NGA group, followed by the GLA group.

Figure 4.2 shows CAPs identified from the left hemisphere monkey data only. The CAPs identified from monkey data show large-scale distributed activations. Further, CAPs are organized in descending order of activation strength, i.e., the amplitude of the activations. These visual patterns were present in all 4 monkeys and provided the means to conveniently categorize the CAPs into different distinct groups for each monkey. The CAPs at the top end for all 4 monkeys (Monkey C: CAPs 9, 3, 8, Monkey G: CAPs 9, 11, 5, Monkey K: CAPs 12, 11, 8, Monkey S: CAPs 1, 12) all have electrode-level z-scores across the whole brain above their average z-score levels (zero) the entire time. This spatial pattern indicates global high activation, making the global high activation (GHA) group. At the bottom end the CAPs (Monkey C: CAPs 2, 4, Monkey G: CAPs 4, 8, Monkey K: CAPs 10, 4, 5, 9, Monkey S: CAPs 8, 4, 2) all have electrode-level z-scores across the whole brain below their average z-score the entire time, indicating global low activations and making this the global low activation (GLA) group. The CAPs having electrode-level z-scores simultaneously above and below their average z-score at separate locations the entire time display a spatial pattern of non-global activation, forming the non-global activation (NGA) group. The analysis of ECoG data was performed independently for each recording for each monkey and led to the same results of classification of CAPs into 3 groups each time analysis was performed across all 4 monkeys. These consistent results indicate the reproducibility of transient brain-wide events and the temporal and transitional traits of the CAPs.

The descending order of activation strength in all 4 monkeys also made it possible to identify 3 distinct CAPs that stood out in the GHA and GLA groups for each monkey and displayed the highest, lowest, and second lowest electrode-level activation within these

groups (Fig. 4.3). The first CAP was considered the highest global activation, identified as CAP 9 in Monkey C and Monkey G, CAP 12 in Monkey K, and CAP 1 in Monkey S, and was termed hCAP. The second CAP was considered the lowest global activation, identified as CAP 4 in Monkey C, CAP 8 in Monkey G, CAP 9 in Monkey K, and CAP 2 in Monkey S, and was termed lCAP. The third unique CAP displayed the second lowest global activation and was termed slCAP. It was identified as CAP 2 in Monkey C, CAP 4 in Monkey G, CAP 5 in Monkey K, and CAP 4 in Monkey S. The existence of these 3 CAPs in different sessions and across different monkeys indicates the reproducibility of their existence and of their unique temporal and transitional patterns.

While brain-wide co-(de)activations are prevalent in CAPs, especially in the GHA and GLA groups, some CAPs in the NGA group especially show regional focus if only looking at co-activation patterns. The CAPs with bilateral frontal co-activations could be identified in the representative results from all four monkeys in Figure 4.2 (Monkey S: CAP10, Monkey C: CAP 8, Monkey G: CAP 12, Monkey K: CAP 6) and in Monkey S in Figure 4.1 (CAP1). Monkey CAPs with bilateral posterior-parietal co-activations in the representative results (Fig. 4.2) are CAP 11 for Monkey S, CAP 5 for Monkeys C and G, and CAP 3 in Monkey K. Bilateral precentral temporal co-activations in the results are seen in CAP 3 for Monkey S, CAP 6 in Monkey G, and CAP 7 in Monkey K in Figure 4.2 and CAP3 for Monkey S (Fig. 4.1). More CAPs with distributed regional focuses of co-activations were consistently identified across different sessions and monkeys, i.e., CAPs showing high co-activations in the temporal and occipital cortices (Monkey S: CAP 1, Monkey G and K: CAP 11), and in the frontal and parietal cortices (Monkey C: CAP 12, Monkey G: CAP 7, and Monkey K: CAP 2).

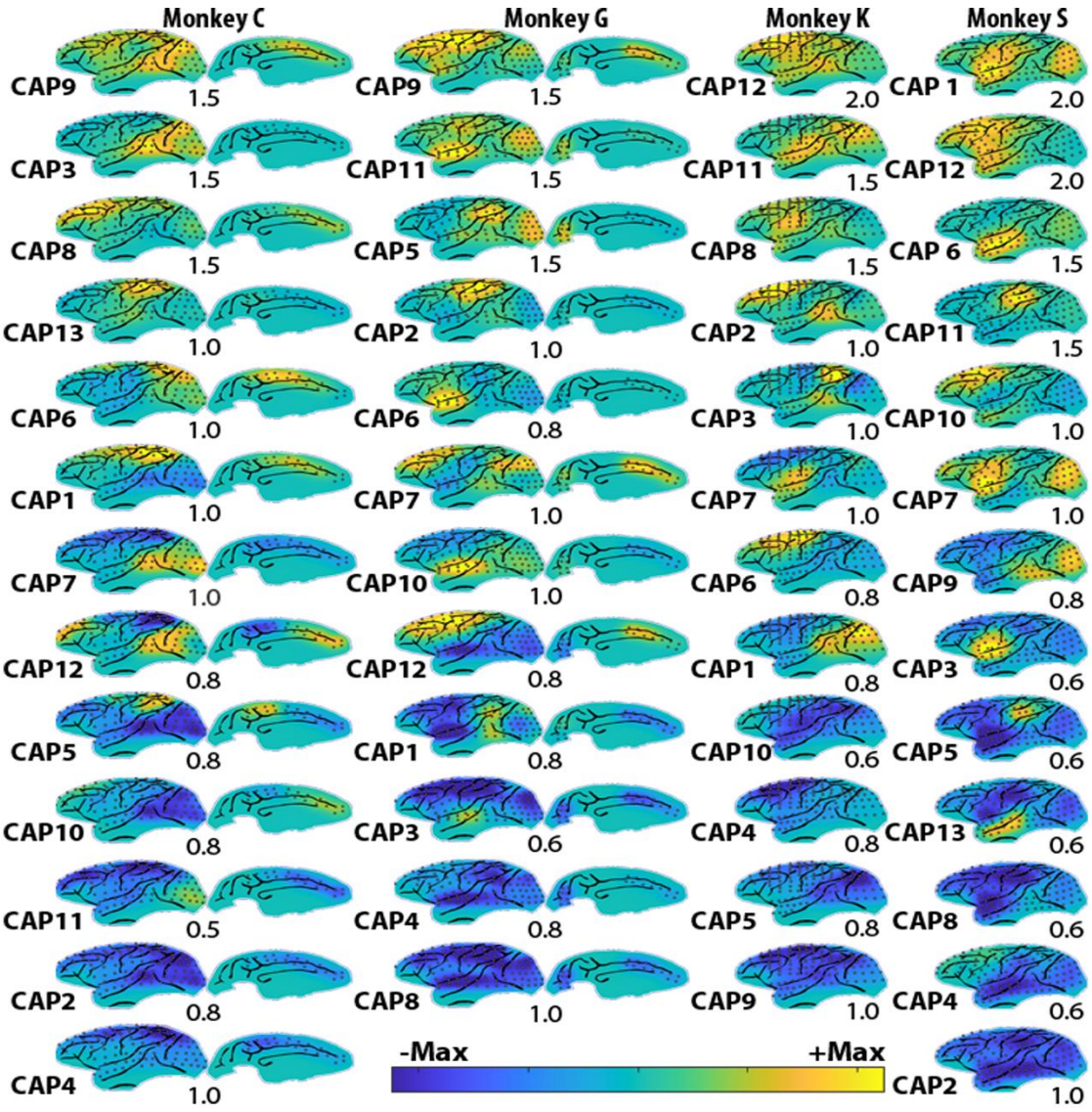


**Figure 4.2.** CAPs for the left hemisphere in all four monkeys. Displayed are the CAPs for each monkey, which were determined by the optimal k-value. The colorbar provided correlates the color to the amplitude of activity, yellow being the highest and blue being the lowest. The CAPs are arranged in descending amplitude of activity. Monkeys C and G are the only monkeys with electrodes implanted on the midline ridge of their left hemisphere.

### 4.2 Temporal Patterns in Monkey ECoG Data

Three metrics were used for group-level (across all datasets for each monkey) monkey ECoG CAPs i.e., occurrence, lifetime, and fractional occupancy (FO). Notable differences were observed for different CAPs or categories of CAPs for monkeys in these metrics (Fig. 4). Among the three categories of CAPs, in general, the CAPs from the GHA group have relatively low occurrences and fractional occupancy rates and the CAPs from the GLA group have relatively high fractional occupancy rates. Slightly higher lifetimes in the CAPs from both the GLA and GHA groups as compared with the CAPs from the NGA group can also be seen. Since the CAPs from the GLA and GHA groups show large variations and are characteristic on these temporal metric values, the reference mean levels of these temporal metrics for each session of monkey data were calculated from the CAPs in the NGA group to be used for statistical comparison with those from individual CAPs, in addition to their direct comparisons between individual CAPs.

The first key observation is that the hCAPs from the monkey data always show significantly lower occurrences than their corresponding lCAPs (Monkey C and G: $p < 0.005$, K: $p < 0.01$, S: $p < 0.05$) and slCAPs (Monkey C, G, and S: $p < 0.005$, K: $p < 0.01$). When compared with the session reference means, all monkey hCAPs (Monkey C, G, and S: $p < 0.005$, K: $p < 0.05$) and most lCAPs (Monkey C and G: $p < 0.005$, S: $p < 0.05$, K: lower but not significant) have significantly lower occurrences. Meanwhile, the occurrences of slCAPs in are always significantly higher than those of the lCAPs (Monkey C, G, and S: $p < 0.005$, K: $p < 0.01$), hCAPs (Monkey C, G, and S: $p < 0.005$, K: $p < 0.01$), and reference means (Monkey C, G, and K: $p < 0.005$, S: $p < 0.01$). Secondly, the hCAPs (Monkey C and G: $p < 0.005$, K, S: $p < 0.01$) and the lCAPs (all $p < 0.005$) from

monkeys have significantly higher mean lifetimes than the reference means while the lifetimes of the most slCAPs show no significant differences as compared with the reference means. Notably, the overall mean lifetimes for monkey CAPs are at the level of 100 milli-seconds. Finally, as the fractional occupancy rates of individual CAPs are determined by both their occurrences and lifetimes, the differences between hCAPs/lCAPs/slCAPs and their respective reference means are enhanced. The FO rates of all hCAPs are significantly lower than the reference means (Monkey C, G, and S: $p < 0.005$, K: $p < 0.05$) and the FO rates of all lCAPs and slCAPs from all monkeys are significantly higher than the reference means (all $p < 0.005$).

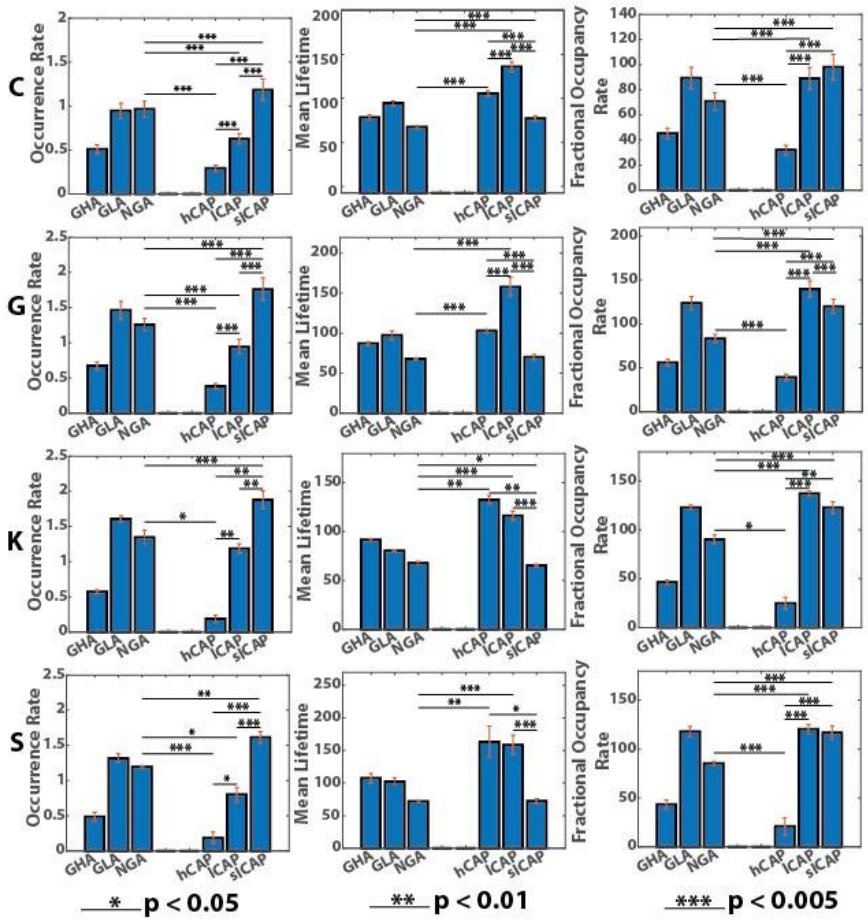


**Figure 4.3.** Temporal metrics of the four monkeys. These plots show the temporal metrics (occurrence rate, mean lifetime, and fractional occupancy rate) for each of the three groups (GHA, GLA, and NGA) and their individual CAPs of importance (hCAP, lCAP, and slCAP) as well as the standard error for each. The means of the CAPs for the grouped data across each session of each monkey was used to form the three groups on the left of the pot. The statistical significance is indicated by asterisk above the bars. P-values were derived from comparing the NGA group with the hCAP, lCAP, and slCAP to emphasize their deviation from the mean, or reference point, of their data, and also from a comparison between the hCAPs, lCAPs, and slCAPs.

### 4.3 Transitional Patterns in Monkey ECoG Data

CAP transitions in monkey data indicate structured patterns that reveal moment-to-moment dynamics between different brain states formed by the entire set of identified CAPs in individual sessions, and these structured patterns are highly supported by the spatial and temporal patterns observed in individual CAPs as discussed in sections 4.1 and 4.2, respectively. Figs. 4.4 and 4.5 illustrated the CAP transition maps (thresholded at > 0.05) from the representative session data from all four monkeys. To better visualize structured transition patterns and the consistencies with their spatial and temporal patterns, the transition rates are coded in the thickness of arrows indicating directed transitions from one CAP to another and the same transition rate data are plotted twice, one with CAP occurrences coded in the size of circles (each represents a CAP, Fig. 4.4) and another one with CAP lifetimes coded in the size of circles (Fig. 4.5). Furthermore, the CAPs from the three categories (i.e., the GHA, GLA, and NGA groups) defined based on their spatial patterns are coded in the color of circles.

These transitions maps suggest the separate roles played by the CAPs from the GHA, GLA, and NGA groups. Firstly, the transitions between the GHA CAPs and the GLA CAPs are mediated by the CAPs from the NGA group: there are no direct transitions between the GHA CAPs and the GLA CAPs in both Figs. 4.4 and 4.5). Secondly, the transitions between all hCAPs and their corresponding lCAPs (e.g., between CAPs 4 and 9 for Monkey C, CAPs 12 and 9 for Monkey K, CAPs 9 and 8 for Monkey G, and CAPs 1 and 2 for Monkey S) indicate the longest paths that usually involve the exploration of multiple other brain states (CAPs) in the middle. These transition paths usually start with the lCAP to other GLA CAP(s), then to NGA CAP (s), then to GHA CAP(s), and ends at

the hCAP. An example of such paths in Fig. 4.4 is: CAP 9 (lCAP) -> CAP 10 (GLA) -> CAP 7 (NGA) -> CAP 8 (GHA) -> CAP 12 (hCAP) for data from Monkey K. Lastly, it is important to note that there are no direct transitions between all hCAPs and their corresponding lCAPs (even after removal of threshold of > 0.05) in all session data (all data listed in Table 1 and beyond the representative examples in Figs. 4.4 and 4.5). These maps show different roles of the GLA, GHA, and NGA CAPs played in transitions among different brain states, which are co-incident with the differences in occurrence and lifetime measures of the CAPs from different categories, e.g., the CAPs with relatively high occurrences appear in the middle of these transition maps while the CAPs with relatively low occurrences are on the boundary of the transition maps. Oppositely, the CAPs with relatively long lifetimes show on the boundary of the transition maps while the CAPs with relatively short lifetimes appear in the middle of the transition maps. In general, lCAPs and hCAPs represent the extreme brain states on the boundary of the transition maps, which both have the lowest occurrences and the longest lifetimes (see details in Fig. 4.3). Furthermore, the slCAPs that have the highest occurrences (Fig. 4.3) are usually in the gateway positions of the corresponding lCAPs to other brain states, e.g., CAP 10 (slCAP) for CAP 9 (lCAP) for Monkey K data (Fig. 4.4).

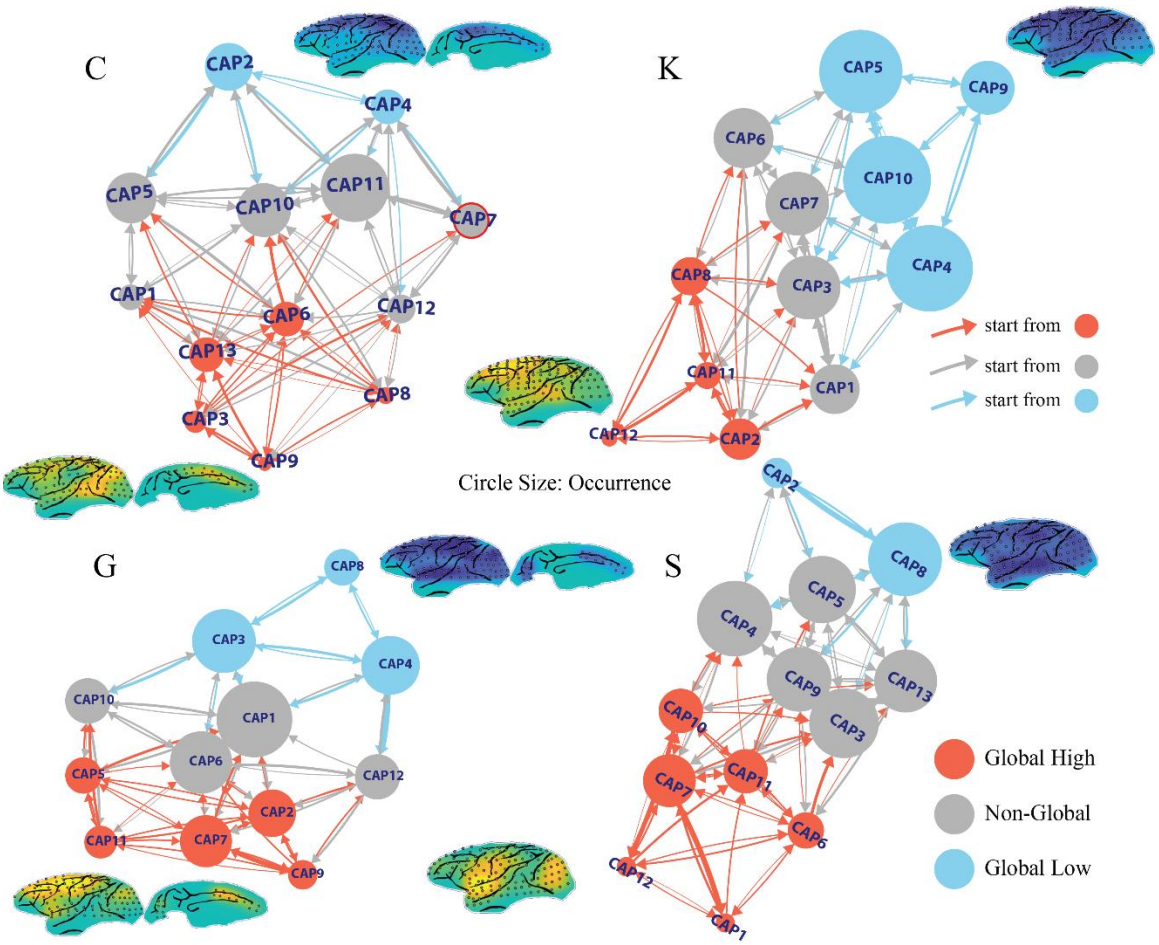


**Figure 4.4.** Occurrence transitional patterns of all four monkeys. The single left hemisphere of each monkey is plotted in reference to the lCAP from the GLA group (blue) and the hCAP of the GHA group (red). Circle sizes provide an indication of the frequency of visits to a specific CAP. Arrows are provided to show the direction in which the CAPs transition between states.

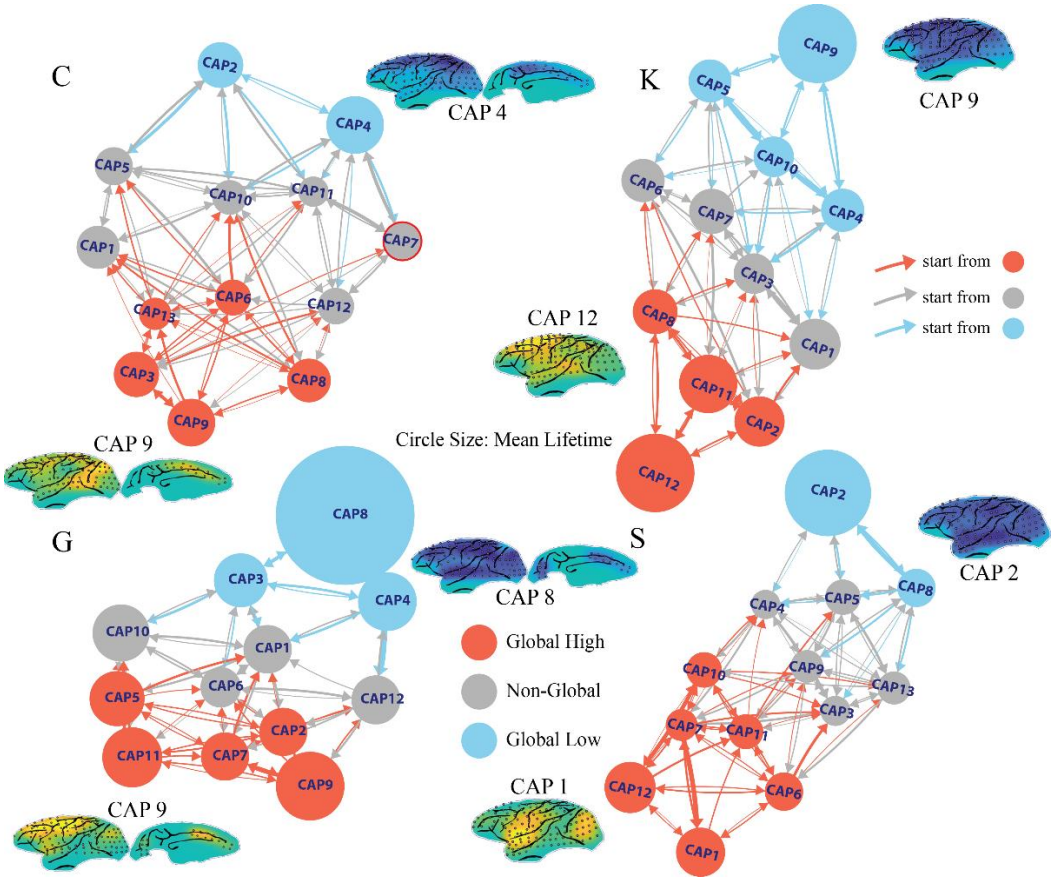


**Figure 4.5.** Lifetime transitional patterns of all four monkeys. Transitional patterns of mean lifetime are displayed for all four monkeys within their left hemisphere. Circle size is indicative of the amount of time spent within each state and arrows are provided to show the direction of the transition between each state. The hCAP and lCAP of each monkey are for a reference to emphasize certain visible patterns observed in the three groups, i.e., GHA in red, GLA in blue, and NGA in gray.

# Chapter 5

## Comparison to Identified Transient Brain-wide CAPs in Human

**5.1 Spatial Patterns**.

For the CAPs identified from human data, brain-wide patterns of large-scale distributed activations could be observed that were like those found in the monkey data (Fig. 5.1B and Fig. 4.2). Furthermore, these CAPs from human data could also be visually conveniently grouped into different categories like those identified in monkeys (see section 4.1). CAPs 5, 6, and 7 from humans (Fig. 5.1A) have all ROI-level z-scores and across the whole brain above their corresponding mean z-score levels of the entire time (which is zero), indicating the global high-activation (the GHA group). CAPs 2, 3, and 8 from human and CAPs 2, 5, and 8 make up the global low-activation (GLA group). CAPs 1 and 4 in humans indicate the patterns of non-global activations (the NGA group). These consistencies of three distinct categories of CAP activation patterns suggest the reproducibility of such transient brain-wide events both within species and across species. CAPs from these three groups further indicate distinct reproducible temporal and transitional characteristics.

Moreover, an arrangement of CAPs in decreasing activation strengths, reflected similarly in both the global activation strength (i.e., sum of ROI over the whole brain) and maximal ROI activation strength (numbers labeled in each CAP spatial map in Figs 5.1 and 4.2), are observed within both GHA and GLA groups in both human and monkey data. For the human GHA group, the order of the amplitudes of activations according to the

global activation strength is CAP 5, 7, then 6. For the GLA group, the order of activation amplitudes is CAP 3, 2, then 8 (fewer negative values mean relatively higher amplitudes due to normalized z-scores). For Monkey S' GHA group (Fig. 5.1A), the order of activation amplitudes is: CAP 12, 4, 13, 10, 3, then 6, while the GLA group's order of activation amplitudes is: CAP 8, 2, then 5. The similar orders of CAPs in each group were also reflected in the maximal ROI/electrode-level activation strength for both human and monkey data. The activation strengths of the CAPs from the NGA groups are in general between those from the GHA and GLA groups (in terms of the maximal ROI/electrode-level activation strength as the global activation strength is expected to be low due to cancellation of positive and negative z-scores in calculating the sum). For the single-hemisphere ECoG data in all four monkeys, similar arrangements of CAP activation strengths between and within three groups are observed (Fig. 4.3). Due to these differences in activation strengths found in human data, the same distinct CAPs to note were the same, i.e., the hCAP (CAP 5 in human and 12 in Monkey S), lCAP (CAP 8 in human and CAP 5 in Monkey S), and slCAP (CAP 2 for human and Monkey S).

The spatial maps of CAPs for human and Monkey S (Fig. 5.1) show another distinct pattern, which is symmetry between two hemispheres. The symmetric pattern is dominant in human CAPs (Fig. 5.1A), while it is also largely present in CAPs from Monkey S (Fig. 5.1B), especially for the CAPs from both the GHA (i.e., CAP 12, 4, 13, and 10) and GLA groups (i.e., CAP 8, 2, and 5). Some CAPs from Monkey S seem not so symmetric visually due to different strengths of co-activation areas (warm colors), but still symmetric in terms of the relative spatial distribution of co-activation and co-deactivation areas (cold colors). For example, CAP 6 presents the general brain-wide symmetry of co-activation and co-

deactivation while the co-activation within the visual cortex of the left hemisphere is weakened. Similarly, CAP 9 presents the general cross-hemisphere symmetry but with weakened co-activations within the left posterior temporal cortex as compared with the corresponding right hemisphere. Some CAPs from Monkey S seem to lose the general brain-wide symmetry of co-activation and co-deactivation but are preserved in a pair of CAPs (like the CAP 7 and 11 pair). It is important to note that the symmetric CAP pairs (one for left hemisphere and one for right hemisphere) could be similarly identified when both-hemisphere data from Monkey S were analyzed separately for left-hemisphere and right-hemisphere (see Fig. 4.1).

Another important observation to note is the presence of CAPs with brain-wide co-(de)activations showing regional focuses. These are emphasized in human data in the same way as the monkey data (see section 4.1), especially if only focusing on coactivations. For example, CAP 1 for humans from the NGA group and CAP 1 for both-hemisphere in Monkey S show high bilateral co-activations within the frontal cortex (Fig. 5.1). Human CAP 4 (Fig. 5.1) from the NGA group and CAP 11 in the left-hemisphere for Monkey S (Fig. 4.2) show high bilateral co-activations within the posterior-parietal cortex. Furthermore, human CAP 1 and Monkey S CAP 3 (Fig. 5.1) shows high bilateral co-activations within the anterior temporal cortex. From representative monkey ECoG data (Fig. 4.2), more CAPs with distributed regional focuses of co-activations could be consistently identified across different sessions and monkeys, as presented in section 4.1.

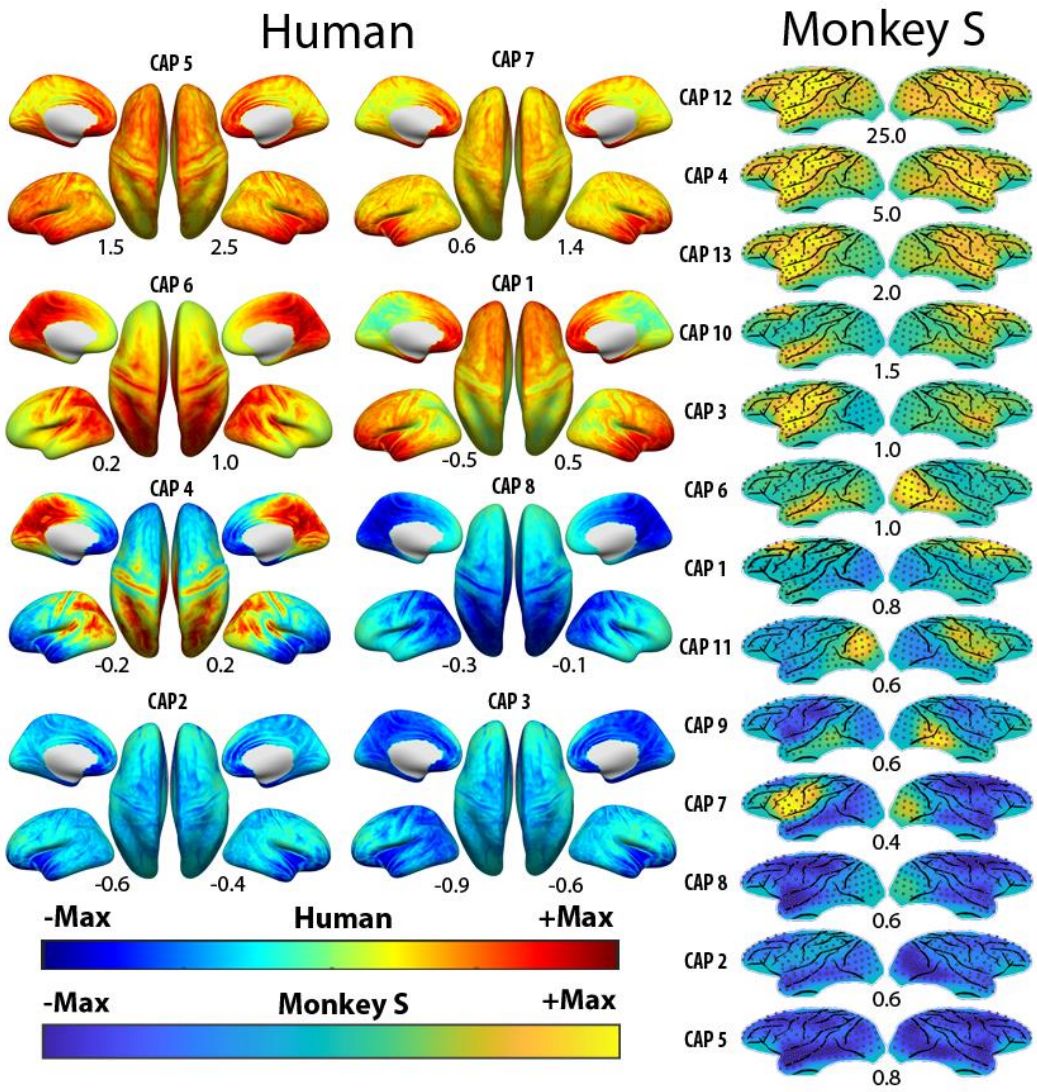


**Figure 5.1.** Human and monkey CAPs for both hemispheres. Human CAPs (8) and CAPs from Monkey S (13) are shown with their corresponding colorbars indicating the amplitude of activity, red having the highest for humans, yellow having the highest for Monkey S, and blue having the lowest for both Monkey S and humans. According to visual inspection of spatial patterns and then arranged in descending order of their activity amplitude, the CAPs are further organized into three distinct groups for Monkey S and humans: global high activation, nonglobal activation, and global low activation. The highest global high activation, CAP 12 for Monkey S and CAP 5 for humans, is at the top, and the secondary global low activation (CAP 2 for Monkey S and humans) and lowest global low activation (CAP 5 for Monkey S and CAP 3 for humans) are at the bottom.

### 5.2 Temporal Patterns

The patterns found in the temporal metrics of monkeys were also similar to those present in human data. The CAPs from the GHA group have relatively low occurrences and fractional occupancy rate and the CAPs from the GLA group have relatively high fractional occupancy rates. The GLA and GHA groups as compared with the CAPs from the NGA group also displayed higher lifetimes than the NGA group. The reference mean levels of the temporal metrics for each participant were calculated in the same manner as the monkey session calculations from the NGA group and were used to statistically compare with the hCAP, lCAP, and slCAP.

One observation is that the hCAP from human always showed a significantly higher occurrence than the corresponding lCAP ($p<0.005$) and slCAP ($p<0.005$). Compared to the participant reference means (NGA group), the hCAP ($p< 0.005$) and lCAP ($p<0.005$) had significantly lower number of occurrences. Observations similar to most lCAPs found in monkeys and all monkey hCAPs. The occurrences of the slCAP were always significantly higher than lCAP's ($p< 0.005$) and reference mean ($p<0.005$), the same significant pattern found in previously mentioned monkey data. Both species also showed the hCAP and lCAP also having significantly higher mean lifetimes than the reference mean and the slCAP having no significant difference when compared to the NGA group mean. Another similarity in the mean lifetimes of the CAPs between monkey and human data was they were on the level of milliseconds. Lastly, the fractional occupancy rate of the hCAP in human were significantly lower than the reference mean ($p < 0.005$), like the findings in monkey data.

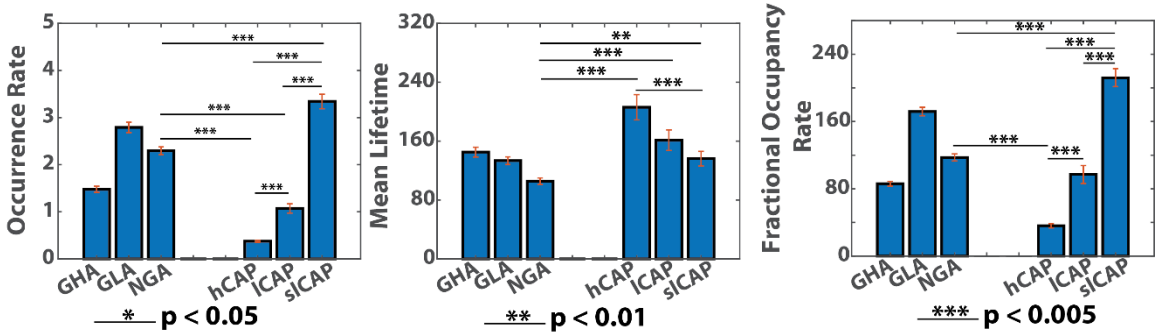


**Figure 5.2.** Temporal metrics of humans. These plots show the temporal metrics (occurrence rate, mean lifetime, and fractional occupancy rate) for humans three groups (GHA, GLA, and NGA) and their individual CAPs of importance (hCAP, lCAP, and slCAP) as well as the standard error for each. The means of the CAPs for the grouped data come from the means across each participant of their associated CAP belonging to that group. The statistical significance is indicated by asterisk above the bars. P-values were derived from comparing the NGA group with the hCAP, lCAP, and slCAP to emphasize their deviations from the mean, or reference point, of their data, and also from a comparison between the hCAPs, lCAPs, and slCAPs.

### 5.3 Transitional Patterns

Supported by spatial and temporal patterns, CAP transitions in human and monkey data show similar structured patterns. These patterns present moment-to-moment dynamics between different brain states formed by all CAPs in each session. Figure 5.4 shows a representative illustration of group level human data and session data from Monkey S. Transitions are coded in the thickness of the arrows that show the direction of the transition between CAPs. These transitions are plotted for both CAP occurrence rates and CAP mean lifetimes. The size of the circles indicates the number of occurrences and the length of the lifetime spent in each state. The CAPs from the GHA, GLA, and NGA groups are represented by the circle color.

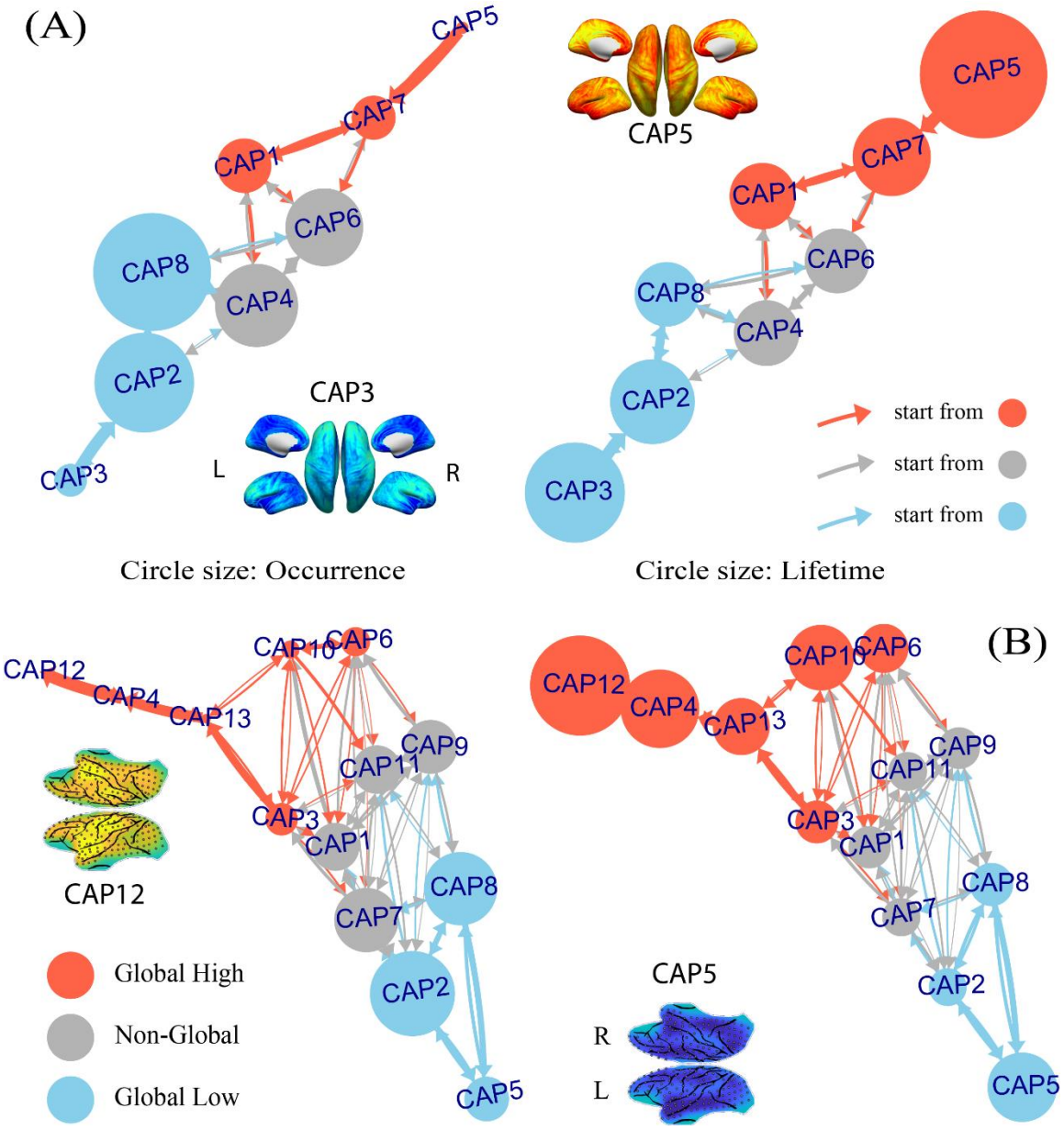


**Figure 5.3.** Occurrence and lifetime transitional patterns of humans and Monkey S. Both hemispheres are displayed for both human and Monkey S of the CAPs corresponding with the hCAP and lCAP visible in the occurrence and lifetime plots. Arrows are used to indicate the direction of transitions between CAPs and circle sizes are indicative to the number of visits to a specific CAP (A) or the duration stayed within each state (B). Colors of the circles indicate which of the three groups the CAP belongs to, i.e., GHA in red, GLA in blue, or NGA in gray.

These transition maps indicate the role of the CAPs in each of the three groups (GLA, GHA, and NGA). Transitions between the GLA and GHA group are always mediated by the NGA group. In other words, there are no direct transition paths between the GLA and GHA group. Further, transitions between two of the extreme CAPs of the GLA and GHA groups (lCAP and hCAP) have the longest paths in which transitions to other CAPs (brain states) must occur. Just like the Monkey data in Figures 4.4 and 4.5, the paths start with the lCAP, moves to other GLA CAP(s), then NGA CAP(s), on to GHA CAP(s), and finally ends at the hCAP. Examples of such paths in Figure 5.4 consist of: CAP 3 (lCAP) -> CAP 2 (GLA) -> CAP 4 (NGA) -> CAP 1 (GHA) -> CAP 7 (GHA) -> CAP 5 (hCAP) for human data and CAP 5 (lCAP) -> CAP 2 (GLA) -> CAP 7 (NGA) -> CAP 1 (NGA) -> CAP 3 (GHA) -> CAP 13 (GHA) -> CAP 4 (GHA) -> CAP 12 (hCAP) for data from Monkey S. Similar to the single hemisphere patterns observed in Figures 4.4 and 4.5, there are no transitions between the hCAP and lCAP in both human data and both hemisphere Monkey S data.

Another key observation is that CAPs with high occurrences and short mean lifetimes are always in the middle of the transition maps. The CAPs at the outer boundaries of the transition maps have few visits to them and the time spent in those states is of long duration. CAPs closest to the boundary, hCAP and lCAP, both have the lowest occurrences and the longest mean lifetimes, according to Figure 5.2 for humans. The slCAP for humans also has the highest number of occurrences (Fig. 5.2) and is usually the entrance for their lCAP to other CAPs. An example of this is CAP 2 (slCAP) being the gateway for CAP 3 (lCAP) for the human data in Figure 5.4A, and CAP 2 (slCAP) for CAP 5 (lCAP) in

Monkey S data in Figure 5.4B. These observations are like the phenomena explored in single hemisphere transition results in Figures 4.4 and 4.5.

### 5.4 Summary of Similarities Between Monkeys and Humans

Key similarities and differences between human CAPs from EEG data and monkey CAPs from ECoG data are summarized in Table 2. These are in comparison between the spatial, temporal, and transitional patterns explained throughout Chapter 5. The comparison resulted in five consistencies within the spatial domain of the two species (human and monkey), six temporal pattern consistencies, and five transitional pattern consistencies. Most of the key similarities are those observed in the differences within members of resultant patterns (hCAP and lCAP), and the low occurrence of the hCAP and high occurrence of the slCAP. However, of the spatial, temporal, and transitional domains, most similarities arise from the temporal and transitional measures. All similarities across all domains presented (spatial, temporal, and transitional) allude to the fact that human EEG CAPs and monkey ECoG CAPs have a strong connection.

**Table 2 Summary of Significant Similarities between Monkey and Human Data.**
This table outlines the many similarities between the human EEG and monkey ECoG data, as described in the results chapter 5.

| Domain of Patterns | Description of Features | Human EEG | Monkey ECoG |
|---|---|---|---|
| Spatial patterns | Three groups: GHA, GLA, and NGA | Yes | Yes, for all monkeys |
| | hCAP and lCAP | Yes | Yes, for all monkeys |
| | Ordered changes of activation strengths across three groups and within groups | Yes | Yes, for all monkeys |
| | Bilateral symmetry | Yes, for all CAPs | Yes, for the majority of CAPs |
| | Regional focuses of co-activations | Several CAPs | More CAPs; CAPs showing similar regional focuses as in human CAPs identified |
| Temporal measures | Low occurrence of hCAP | Yes | Yes |
| | High occurrence of slCAP | Yes | Yes |
| | Long lifetime of hCAP and lCAP | Yes | Yes |
| | Low FO for hCAP | Yes | Yes |
| | High FO for slCAP | Yes | Yes |
| | Overall mean lifetime | ~150 ms | ~150 ms |
| Transitional patterns | hCAPs and lCAPs at the two ends of the transition maps | Yes | Yes |
| | No direct transition between the CAPs from GHA and the CAPs from GLA. | Yes | Yes |
| | Transitions between hCAP and lCAP mediated by other CAPs in GHA and GLA groups | Yes | Yes, for the majority of session data for all monkeys |
| | Low/high occurrences for CAPs at the end/middle of transition maps | Yes | Yes |
| | Long/short lifetime for CAPs at the end/middle of transition maps | Yes | Yes |

# Chapter 6

## Comparison of Phenomena Between Anesthesia and Resting Monkey ECoG Data

After analyzing ECoG data under resting conditions of monkeys and comparing the results to human resting EEG data, I was able to find many similarities between not only two different species, but between differing imaging modalities used for each species as well. Upon completion of these initial goals one question remained pertaining to different states of consciousness of the same species with data from the same imaging modality. To accomplish this final goal the same experimental methods implemented for analysis of monkey ECoG resting state data were used to process and analyze ECoG anesthetized state data from the same monkeys.

### 6.1 Spatial Patterns in Anesthesia Monkey Data

Visual inspection of the spatial maps of the anesthesia data, i.e., ketamine-medetomidine (KTMD) anesthetic agents used simultaneously for all monkeys showed the same consistent patterns, so there was an assumption made that any one monkey's spatial map of their CAPs was representative of all four monkeys under the same condition. All anesthesia sessions also revealed almost identical patterns even with different types of anesthetics used in the session for all monkeys, however the most consistent results came from the KTMD sessions for all four monkeys. For this reason, the KTMD of Monkey G was used to represent all monkeys. Monkey G revealed similar patterns as those found in the spatial maps from the resting awake condition in that large-scale distributed activations were also present in the anesthesia data (Fig. 6.1). With these similarities, I could also categorize the CAPs into three groups (GLA, GHA, and NGA groups). I was also able to

identify CAPs on the extreme end of the GLA group (lCAP) as well as the GHA group (hCAP). Further, I was also able to identify the slCAP of the GLA group. The CAPs in Figure 6.1 are arranged in descending order of activation strength, with the GHA group on top, NGA group in the middle, and GLA group on bottom. In Monkey G, CAPs 12, 4, 10, and 11 make up the GHA group with CAP12 being the hCAP, and CAPs 6 and 3 make up the GLA group with CAP 3 and CAP 6 being the lCAP and slCAP, respectively.

Another consistent result with the anesthesia and resting sessions of Monkey G were in the regional focuses of the coactivations. There was bilateral posterior-parietal focus observed in CAP 2, bilateral precentral temporal in CAP 5, and bilateral frontal activations in CAP 8.

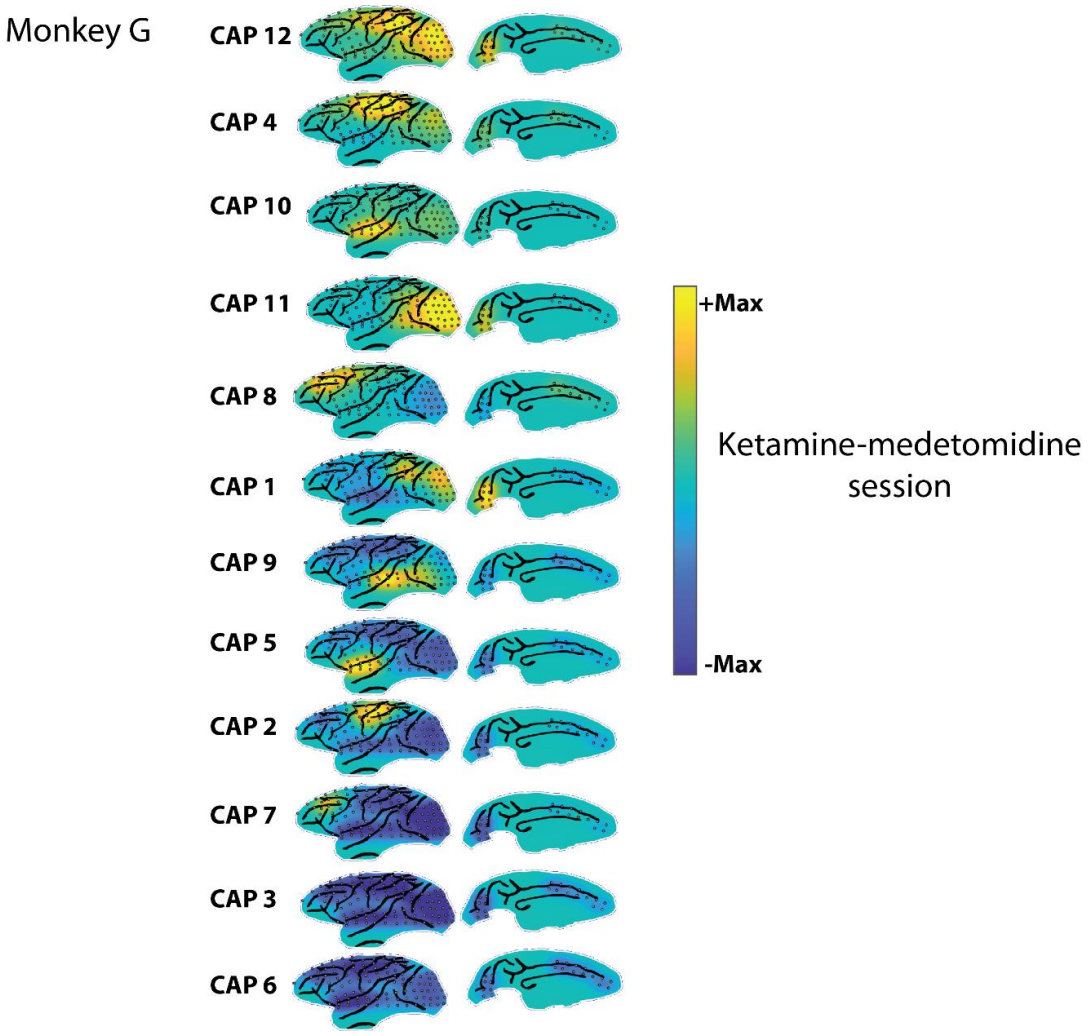


**Figure 6.1**. Spatial map of Monkey G. The CAPs from a single session of anesthesia (KTMD) data from Monkey G are presented. They are arranged in descending order of activity amplitude starting with the hCAP from the GHA group at the top, then the NGA group, and finally the lCAP from the GLA group at the bottom.

### 6.2 Temporal Patterns in Anesthesia Monkey Data

General temporal patterns (Fig. 6.2) also proved to be consistent between resting and anesthetized monkeys. The metrics used were the ones corresponding to a single KTMD anesthesia session with Monkey G's spatial map of ECoG CAPs displayed in Figure 6.1. These consisted of occurrence rate, mean lifetime, and FO rate. The hCAP from the anesthesia data has a relatively low occurrence and FO rate. Again, slightly higher lifetimes were found in the slCAP group and hCAP group from the anesthesia data when compared to the lCAP group from the GLA group. The lCAP group and slCAP group also had a higher number of occurrences than the hCAP group.

Although the general patterns were found to be similar there were significant differences in the actual number of occurrences, length of mean lifetimes, and actual FOs of the hCAPs between the anesthesia and resting conditions. Figure 6.3 uses group-level session data for direct comparison of the resting CAPs and anesthesia CAPs of all four monkeys. This group-level was across all KTMD anesthesia sessions of all four monkeys, the metrics were then averaged and displayed along with the standard error across all datasets from all monkeys. The resting data consisted of the extracted resting portion of these same KTMD sessions in all four monkeys, and then the lifetimes, occurrences, and occupancies were also averaged with the same procedure used for the anesthesia data. The hCAPs from the anesthesia data had significantly lower occurrences ($p < 0.005$) and FOs ($p < 0.05$) than the hCAPs from the resting data, and they had significantly higher mean lifetimes ($p < 0.005$) than the hCAPs from the resting data (Fig. 6.3). The lifetimes of the slCAPs were also significantly higher for the anesthesia data than the resting ($p < 0.05$),

and the lCAPs for FO were also significantly higher in the anesthesia data than the resting ($p < 0.05$).

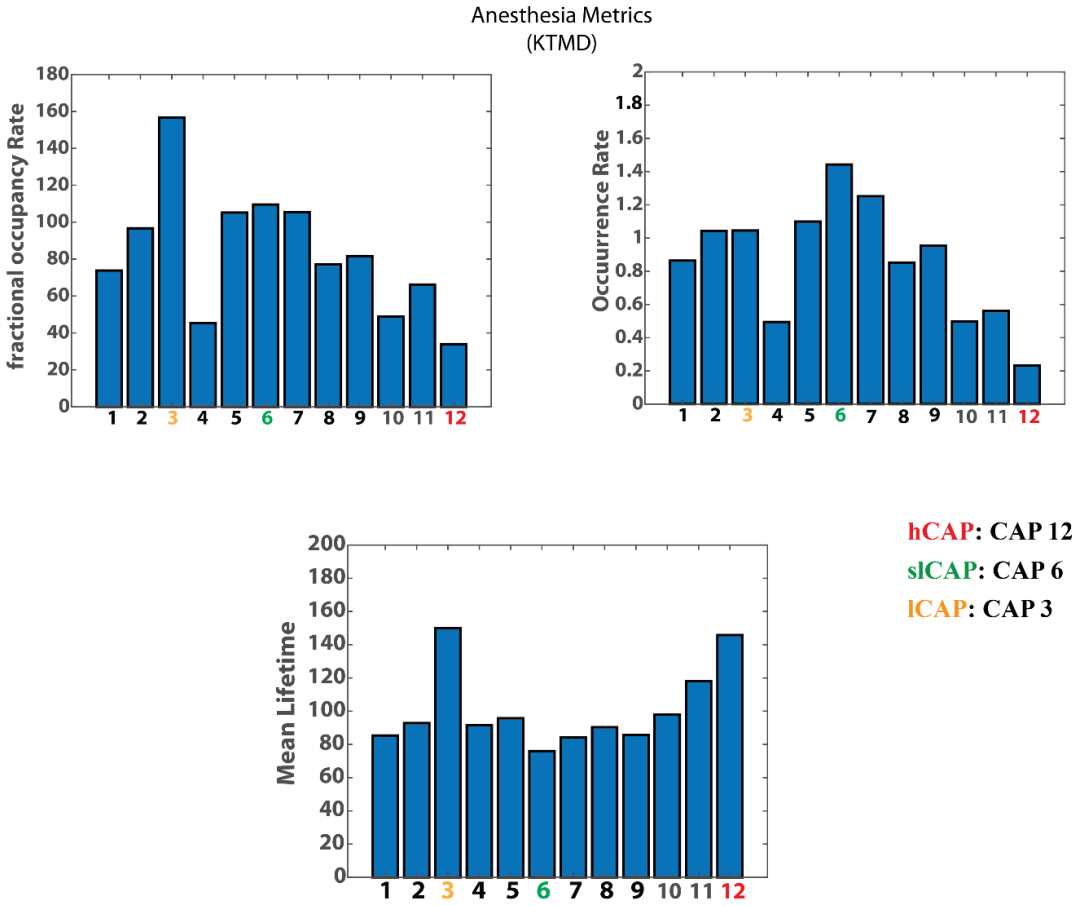


**Figure 6.2**. Metrics for Monkey G anesthesia. The FO, occurrences, and lifetime metrics are all displayed here for one anesthesia session of Monkey G. The hCAP, lCAP, and slCAP, CAP 12, CAP 6, and CAP 3, respectively, are emphasized to display their corresponding characteristics.

### 6.3 Key Observed Similarities/Differences

Comparison of the resting and anesthetized brain states revealed many similarities between them within their spatial and temporal patterns (Figs. 6.1 and 6.2). Though the trends were consistently similar, there were significant differences in the actual number of occurrences, length of mean lifetimes, and occupancies of the hCAP, lCAP, and slCAP groups. In summary, these significant differences were largely found in the hCAP group in all three metrics (occurrences, lifetimes, occupancies). Figure 6.3 shows the significant differences between the averaged mean lifetimes across each ketamine-medetomidine session for all four monkeys with those averaged from the resting portion of the same datasets. It is also important to note that these results are preliminary, and therefore more analysis would be required to fully support these conclusions.

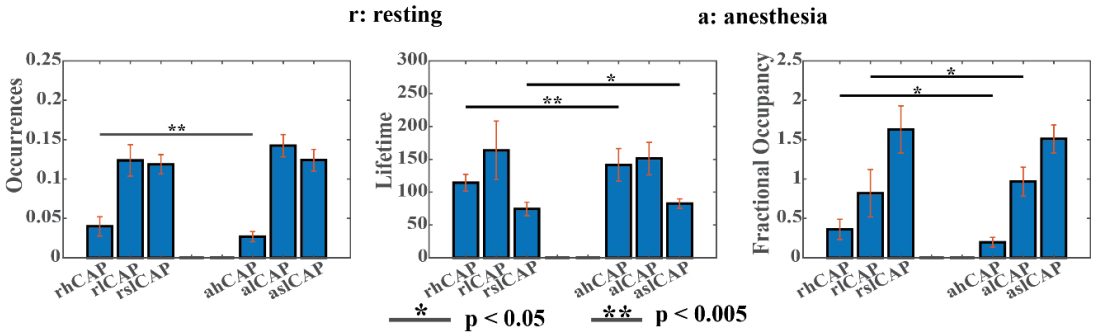


**Figure 6.3.** Average of metrics for anesthetized (KTMD) monkeys. Here is shown the occurrences, lifetimes, and occupancy of all four monkeys extracted from their anesthesia data. The k-value used was 12 for each monkey and lifetime was extracted then averaged across all sessions of the ketamine-medetomidine (Monkey C: 2 sessions, Monkeys G, K, and S: 3 sessions). Error bars have been provided.

# Chapter 7

# Discussion

## 7.1 Discoveries and Comparison to Literature

After identifying the existence of transient brain-wide coactivation patterns (CAPs) in monkey ECoG data, resting and anesthesia, I observed many spatial, temporal, and transitional patterns. These patterns were also present in another study (Ding et al., 2022). This study not only identified CAPs in human resting data, but also explored what they defined as the 'superstructure' (Ding et al., 2022), which they hypothesized as the potential driver to the similarities that exist in both human and monkeys and governs the brain-wide CAP dynamics. This structure is defined by the two polarized CAPs with intermediate states in between them, i.e., the hCAP and lCAP within the global high activation (GHA) and global low activation (GLA) groups that border the nonglobal activation group (NGA). The structure is additionally defined by the temporal and transitional behavior of the identified CAPs: fewer visits to the polarized CAPs (low occurrence of the hCAP and lCAP), and transitions between these polarized states always being mediated by the intermediate CAPs without a direct transition between the two (intermediate states have more visits and for shorter periods of time). The results of monkey ECoG resting state data analysis in this research show promising in how similar they are to those found in humans in both this study and the before mentioned study (Ding et al., 2022). The correspondence of these results (transient events) in both human and monkeys further validates the existence of brain-wide patterns retained in evolution.

Furthermore, previous studies have supported the results of this research, specifically the similar patterns in the resting and anesthesia state in monkey ECoG data coincide with results of other studies (Mantini et al., 2011, Vincent et al., 2007). This research group was able to find analogous connections in brain activity between monkeys and humans in different levels of consciousness, i.e., awake and unconsciousness induced by anesthesia (Mantini et al., 2011, Vincent et al., 2007).

### 7.2 Conclusion

Analysis of electrophysiological neural signals measured by EEG and ECoG neuroimaging methods provided results I was able to use to compare brain-wide patterns across different species (humans and monkeys) and different state of consciousness within the same species. CAPs were able to be identified in monkey ECoG data after cluster analysis was performed, which were similar to those found in human EEG data. Spatial, temporal, and transitional metrics from neural networks were compared and patterns known to be preexisting and thought of as unique only in humans were also reflected in monkeys. These brain-wide coactivation patterns and their metric characteristics in the resting state of monkeys were also revealed to exist in anesthesia conditions of monkeys. Consistent with what is expected, there were differences in the different states of consciousness in that there were significant differences between the hCAP groups of the three metrics between monkey resting and anesthesia states in the magnitude of the metrics.

The significant similarities between human and monkey resting data, along with the expected differences found between the different states of consciousness in the monkey data further validate the results of this study.

### 7.3 Summary

In this research I sought out to determine the existence of transient brain-wide coactivation patterns in macaque monkeys, observe any spatial, temporal, and transitional similarities between the monkeys and humans as well as any similarities within different states of consciousness in monkeys using EEG and ECoG data analysis to investigate. I was able to positively identify the existence of these CAPs and made a comparison between human and monkey neural activations to determine if there were any patterns that could be identified between the monkeys and humans in their resting states. Furthermore, using visual inspection of their spatial maps I was able to their large-scale distributed activity patterns to separate the CAPs of both humans and monkeys into three groups, i.e., global high activation, global low activation, and nonglobal activation groups. The comparison between the two species (monkey and human) for the whole brain could only be made between Monkey S and humans because only Monkey S had both hemispheres of information with the other three monkeys only having the left hemisphere. One key observation made was the symmetry in neural activity on the spatial maps between the right and left hemisphere of both the human and monkey brains as well as regional focuses. Furthermore, arranging the CAPs in decreasing activation strength, three CAPs were particularly noted in both the human's and monkey's GLA and GHA group (hCAP, lCAP, and slCAP). Using the similarities reflected across both hemispheres in humans and Monkey S an assumption was made that the left hemisphere of the other three monkeys was indicative of what the right hemisphere activity would be. I was able to compare all four monkeys to human data based off this assumption.

Not only were similar spatial patterns observed between humans and monkeys, but their temporal and transitional metrics were found to be similar to humans. One important temporal pattern to note was the hCAP always had the lowest fractional occupancy and occurrence rate with a high mean lifetime. Another important observation was that the slCAP always had the highest occurrence rate. Finally, the slCAP and the lCAP both had high mean lifetimes and fractional occupancy. Transitional patterns include the direction of transitions between states (CAPs) and the amount of time or the frequency of occurrences of each state. Transitions never occurred directly between the GHA group and the GLA group and mediation was always through the NGA group. The hCAPs and lCAPs also had very few visits but the time spent in these states was always long. The CAPs within the middle of the transition maps (Figs. 5, 6, Supplementary Fig. 3) always had a higher number of occurrences than those towards the boundaries. In other words, the most visits occurred in the NGA groups with the least occurring in the GLA and GLA groups. Transitions between the hCAPs and lCAPs always had the longest paths with visits to the NGA CAPs along the way. These same analysis methods were further used to compare monkeys in their resting state to their anesthetized state. Visualization of spatial maps and results found in the analysis of electrophysiological signals of the monkeys in these different brain states revealed many consistencies between their spatiotemporal and transitional patterns. The one difference of importance to note was the average duration of lifetime for CAPs. The mean lifetime of the resting state CAPs was generally shorter than those in the anesthetized state (see section 6.2).

Moreover, it is important to note that similarities found between humans and monkeys were derived from different modalities of neural imaging, i.e., EEG for humans

and ECoG for monkeys. All similar patterns revealed were identified using independent processing and analysis of each dataset for each monkey and human.

Similarities identified between human and monkey resting data were also identified between monkey resting data and monkey anesthesia data. These included all spatial, temporal, and transitional patterns discussed in Chapter 4 with a difference in the magnitude of these metrics. These results imply a there exists a difference in brain activity between a conscious resting state and an induced unconscious state within the same species.

### 7.4 Limitations and Future Studies

The number of datasets were limited in this research and were provided from only four monkeys, a small sample size that could potentially not be representative of all macaque monkeys. Not only this but only one monkey had both hemispheres available to analyze, the other three had just the left hemisphere, so there was an assumption that the left hemisphere was representative of neural activity occurring in the right hemisphere. This assumption could bias the results. Only two datasets (one each from Monkey C and Monkey S) contained only resting in their session, the rest of the datasets from all four monkeys had to have the resting portion extracted due to the sessions also involving sleep and anesthesia trials. Resting portions were only taken before these trials were initiated. The resting intervals were conservatively extracted from the datasets but there is still the potential that the extracted data could contain information from the sleep or anesthesia states within the session that overlapped with them. This research also used data from two different neuroimaging methods (EEG and ECoG), which have different spatial and temporal resolutions. These differences stem from the location in which measurements are

taken, on the scalp for EEG and the cortical surface for ECoG. The interference from the scalp smears the data in that the activations are less distinct, leading to fewer clusters of which could explain why the optimal number of clusters to use were different between the human data and monkey data.

Moving forward to future studies, more comparisons could be made between human and monkey data coming from the same neuroimaging modality that could measure primary neural responses (just EEG or just ECoG). Further studies could also include a more in-depth analysis of brain-wide coactivations in monkeys in different states of consciousness, i.e., awake and resting, task-based, sleep, and anesthetized. While I was able to compare between resting and anesthetized sessions, I had limited data to use as well as only using anesthesia data from one monkey instead of all four used in Chapter 4. Given data from humans under anesthesia, a direct comparison to the response of this stimuli could be made between the two species (human and monkey). This could further cement a relation between neural activity in humans and monkeys, providing more support for use of a monkey model for research on the interaction with pharmaceuticals and disease states with the brain with a more invasive means.

# References


ABBAS, A., BELLOY, M., KASHYAP, A., BILLINGS, J., NEZAFATI, M., SCHUMACHER, E. H. & KEILHOLZ, S. 2019. Quasi-periodic patterns contribute to functional connectivity in the brain. *Neuroimage,* 191**,** 193-204.

ARFANAKIS, K., CORDES, D., HAUGHTON, V. M., MORITZ, C. H., QUIGLEY, M. A. & MEYERAND, M. E. 2000. Combining independent component analysis and correlation analysis to probe interregional connectivity in fMRI task activation datasets. *Magn Reson Imaging,* 18**,** 921-30.

ASANO, E., JUHASZ, C., SHAH, A., SOOD, S. & CHUGANI, H. T. 2009. Role of subdural electrocorticography in prediction of long-term seizure outcome in epilepsy surgery. *Brain,* 132**,** 1038-47.

AUER, D. P. 2008. Spontaneous low-frequency blood oxygenation level-dependent fluctuations and functional connectivity analysis of the 'resting' brain. *Magn Reson Imaging,* 26**,** 1055-64.

BAILLET, S., MOSHER, J., LEAHY, R. 2001. Electromagnetic brain mapping. *IEEE Signal Proc Mag,* 18**,** 14-30.

BAKER, A. P., BROOKES, M. J., REZEK, I. A., SMITH, S. M., BEHRENS, T., PROBERT SMITH, P. J. & WOOLRICH, M. 2014. Fast transient networks in spontaneous human brain activity. *Elife,* 3**,** e01867.

BECKER, R. & HERVAIS-ADELMAN, A. 2020. Resolving the Connectome, Spectrally-Specific Functional Connectivity Networks and Their Distinct Contributions to Behavior. *eNeuro,* 7.

BETZEL, R. F., MEDAGLIA, J. D., KAHN, A. E., SOFFER, J., SCHONHAUT, D. R. & BASSETT, D. S. 2019. Structural, geometric and genetic factors predict interregional brain connectivity patterns probed by electrocorticography. *Nat Biomed Eng,* 3**,** 902-916.

BLUME, W. & HOLLOWAY, G. 2011. Electrocorticography. *Extratemporal lobe epilepsy surgery. Surrey, John Libbey***,** 345-351.

BRANCO, M. P., GEUKES, S. H., AARNOUTSE, E. J., RAMSEY, N. F. & VANSTEENSEL, M. J. 2023. Nine decades of electrocorticography: A comparison between epidural and subdural recordings. *Eur J Neurosci,* 57**,** 1260-1288.

BROOKES, M. J., WOOLRICH, M., LUCKHOO, H., PRICE, D., HALE, J. R., STEPHENSON, M. C., BARNES, G. R., SMITH, S. M. & MORRIS, P. G. 2011. Investigating the electrophysiological basis of resting state networks using magnetoencephalography. *Proc Natl Acad Sci U S A,* 108**,** 16783-8.

CHEN, Y., CHA, Y. H., LI, C., SHOU, G., GLEGHORN, D., DING, L. & YUAN, H. 2019. Multimodal Imaging of Repetitive Transcranial Magnetic Stimulation Effect on Brain Network: A Combined Electroencephalogram and Functional Magnetic Resonance Imaging Study. *Brain Connect,* 9**,** 311-321.

COHEN, D. & CUFFIN, B. N. 1983. Demonstration of useful differences between magnetoencephalogram and electroencephalogram. *Electroencephalogr Clin Neurophysiol,* 56**,** 38-51.

CORDES, D., HAUGHTON, V. M., ARFANAKIS, K., WENDT, G. J., TURSKI, P. A., MORITZ, C. H., QUIGLEY, M. A. & MEYERAND, M. E. 2000. Mapping functionally related regions of brain with functional connectivity MR imaging. *AJNR Am J Neuroradiol,* 21**,** 1636-44.

CRONE, N. E., MIGLIORETTI, D. L., GORDON, B. & LESSER, R. P. 1998. Functional mapping of human sensorimotor cortex with electrocorticographic spectral analysis. II. Event-related synchronization in the gamma band. *Brain,* 121 ( Pt 12)**,** 2301-15.

CUSTO, A., VAN DE VILLE, D., WELLS, W. M., TOMESCU, M. I., BRUNET, D. & MICHEL, C. M. 2017. Electroencephalographic Resting-State Networks: Source Localization of Microstates. *Brain Connect,* 7**,** 671-682.

DAITCH, A. L., SHARMA, M., ROLAND, J. L., ASTAFIEV, S. V., BUNDY, D. T., GAONA, C. M., SNYDER, A. Z., SHULMAN, G. L., LEUTHARDT, E. C. & CORBETTA, M. 2013. Frequency-specific mechanism links human brain networks for spatial attention. *Proc Natl Acad Sci U S A,* 110**,** 19585-90.

DARVAS, F., PANTAZIS, D., KUCUKALTUN-YILDIRIM, E. & LEAHY, R. M. 2004. Mapping human brain function with MEG and EEG: methods and validation. *Neuroimage,* 23 Suppl 1**,** S289-99.

DE SALLES, A. A., SWARTZ, B. E., LEE, T. T. & DELGADO-ESCUETA, A. V. 1994. Subdural recording and electrical stimulation for cortical mapping and induction of usual seizures. *Stereotact Funct Neurosurg,* 62**,** 226-31.

DELORME, A. & MAKEIG, S. 2004. EEGLAB: an open source toolbox for analysis of single-trial EEG dynamics including independent component analysis. *J Neurosci Methods,* 134**,** 9-21.

DIEHL, B. & LUDERS, H. O. 2000. Temporal lobe epilepsy: when are invasive recordings needed? *Epilepsia,* 41 Suppl 3**,** S61-74.

DING, L. 2009a. Dynamic connectivity map on ECoG: a new computed signature in defining epileptogenic zone. *Clin Neurophysiol,* 120**,** 1419-21.

DING, L. 2009b. Reconstructing cortical current density by exploring sparseness in the transform domain. *Phys Med Biol,* 54**,** 2683-97.

DING, L., AND YUAN, H. 2012. Inverse source imaging methods in recovering distributed brain sources. *Biomedical Engineering,* 2**,** 2-7.

DING, L. & HE, B. 2008. Sparse source imaging in electroencephalography with accurate field modeling. *Hum Brain Mapp,* 29**,** 1053-67.

DING, L., LAI, Y. & HE, B. 2005. Low resolution brain electromagnetic tomography in a realistic geometry head model: a simulation study. *Phys Med Biol,* 50**,** 45-56.

DING, L., NI, Y., SWEENEY, J. & HE, B. 2011. Sparse cortical current density imaging in motor potentials induced by finger movement. *J Neural Eng,* 8**,** 036008.

DING, L., SHOU, G., CHA, Y. H., SWEENEY, J. A. & YUAN, H. 2022. Brain-wide neural co-activations in resting human. *Neuroimage,* 260**,** 119461.

FISCHL, B. 2012. FreeSurfer. *Neuroimage,* 62**,** 774-81.

FOX, M. D. & RAICHLE, M. E. 2007. Spontaneous fluctuations in brain activity observed with functional magnetic resonance imaging. *Nat Rev Neurosci,* 8**,** 700-11.

FOX, M. D., SNYDER, A. Z., ZACKS, J. M. & RAICHLE, M. E. 2006. Coherent spontaneous activity accounts for trial-to-trial variability in human evoked brain responses. *Nat Neurosci,* 9**,** 23-5.

GEDDES, L. A., HODGE, C. 1996. The retrospectroscope electrocorticography. *IEEE Engineering in Medicine and Biology Magazine,* 15**,** 101-103.

GOZZI, A. & SCHWARZ, A. J. 2016. Large-scale functional connectivity networks in the rodent brain. *Neuroimage,* 127**,** 496-509.

GREICIUS, M. D., KRASNOW, B., REISS, A. L. & MENON, V. 2003. Functional connectivity in the resting brain: a network analysis of the default mode hypothesis. *Proc Natl Acad Sci U S A,* 100**,** 253-8.

GU, Y., SAINBURG, L. E., KUANG, S., HAN, F., WILLIAMS, J. W., LIU, Y., ZHANG, N., ZHANG, X., LEOPOLD, D. A. & LIU, X. 2021. Brain Activity Fluctuations Propagate as Waves Traversing the Cortical Hierarchy. *Cereb Cortex,* 31**,** 3986-4005.

GUNDUZ, A., BRUNNER, P., DAITCH, A., LEUTHARDT, E. C., RITACCIO, A. L., PESARAN, B. & SCHALK, G. 2012. Decoding covert spatial attention using electrocorticographic (ECoG) signals in humans. *Neuroimage,* 60**,** 2285-93.

HAAS, L. F. 2003. Hans Berger (1873-1941), Richard Caton (1842-1926), and electroencephalography. *J Neurol Neurosurg Psychiatry,* 74**,** 9.

HAMALAINEN, M. S. & ILMONIEMI, R. J. 1994. Interpreting magnetic fields of the brain: minimum norm estimates. *Med Biol Eng Comput,* 32**,** 35-42.

HAMPSON, M., PETERSON, B. S., SKUDLARSKI, P., GATENBY, J. C. & GORE, J. C. 2002. Detection of functional connectivity using temporal correlations in MR images. *Hum Brain Mapp,* 15**,** 247-62.

HE, B., DING, L., AND SOHRABPOUR, ABBAS 2020. Electrophysiological Mapping and Source Imaging. *In:* HE, B. (ed.) *Neural Engineering.* 3rd ed.: Kluwer Academic/Plenum Publishers.

HILL, N. J., GUPTA, D., BRUNNER, P., GUNDUZ, A., ADAMO, M. A., RITACCIO, A. & SCHALK, G. 2012. Recording human electrocorticographic (ECoG) signals for neuroscientific research and real-time functional cortical mapping. *J Vis Exp*.

HIPP, J. F., HAWELLEK, D. J., CORBETTA, M., SIEGEL, M. & ENGEL, A. K. 2012. Large-scale cortical correlation structure of spontaneous oscillatory activity. *Nat Neurosci,* 15**,** 884-90.

HUTCHISON, R. M. & EVERLING, S. 2012. Monkey in the middle: why non-human primates are needed to bridge the gap in resting-state investigations. *Front Neuroanat,* 6**,** 29.

HUTCHISON, R. M., LEUNG, L. S., MIRSATTARI, S. M., GATI, J. S., MENON, R. S. & EVERLING, S. 2011. Resting-state networks in the macaque at 7 T. *Neuroimage,* 56**,** 1546-55.

KHAN, A. F., ZHANG, F., SHOU, G., YUAN, H. & DING, L. 2022. Transient brain-wide coactivations and structured transitions revealed in hemodynamic imaging data. *Neuroimage,* 260**,** 119460.

KHODAGHOLY, D., GELINAS, J. N., ZHAO, Z., YEH, M., LONG, M., GREENLEE, J. D., DOYLE, W., DEVINSKY, O. & BUZSAKI, G. 2016. Organic electronics for high-resolution electrocorticography of the human brain. *Sci Adv,* 2**,** e1601027.

KRINGELBACH, M. L. & DECO, G. 2020. Brain States and Transitions: Insights from Computational Neuroscience. *Cell Rep,* 32**,** 108128.

KURUVILLA, A. & FLINK, R. 2003. Intraoperative electrocorticography in epilepsy surgery: useful or not? *Seizure,* 12**,** 577-84.

LAI, D., ZHANG, X., CHEN, W., ZHANG, H., KANG, T., YUAN, H., DING, L. 2020. Channel-wise characterization of high frequency oscillations for automated identification of the seizure onset zone by using machine learning approach in epilepsy. *IEEE Access,* 8**,** 45531-45543.

LAI, D., ZHANG, X., MA, K., CHEN, Z., CHEN, W., ZHANG, H., YUAN, H., DING, L. 2019. Automated detection of high frequency oscillations in intracranial EEG using the combination of short-time energy and convolutional neural networks. *IEEE Access,* 7**,** 82501-82511.

LAI, Y., VAN DRONGELEN, W., DING, L., HECOX, K. E., TOWLE, V. L., FRIM, D. M. & HE, B. 2005. Estimation of in vivo human brain-to-skull conductivity ratio from simultaneous extra- and intra-cranial electrical potential recordings. *Clin Neurophysiol,* 116**,** 456-65.

LEE, M. H., SMYSER, C. D. & SHIMONY, J. S. 2013. Resting-state fMRI: a review of methods and clinical applications. *AJNR Am J Neuroradiol,* 34**,** 1866-72.

LESSER, R. P., CRONE, N. E. & WEBBER, W. R. S. 2010. Subdural electrodes. *Clin Neurophysiol,* 121**,** 1376-1392.

LIAO, K., ZHU, M. & DING, L. 2013. A new wavelet transform to sparsely represent cortical current densities for EEG/MEG inverse problems. *Comput Methods Programs Biomed,* 111**,** 376-88.

LIAO, K., ZHU, M., DING, L., VALETTE, S., ZHANG, W. & DICKENS, D. 2012. Sparse imaging of cortical electrical current densities via wavelet transforms. *Phys Med Biol,* 57**,** 6881-901.

LIU, X., CHANG, C. & DUYN, J. H. 2013. Decomposition of spontaneous brain activity into distinct fMRI co-activation patterns. *Front Syst Neurosci,* 7**,** 101.

LIU, X. & DUYN, J. H. 2013. Time-varying functional network information extracted from brief instances of spontaneous brain activity. *Proc Natl Acad Sci U S A,* 110**,** 4392-7.

LIU, X., YANAGAWA, T., LEOPOLD, D. A., FUJII, N. & DUYN, J. H. 2015. Robust Long-Range Coordination of Spontaneous Neural Activity in Waking, Sleep and Anesthesia. *Cereb Cortex,* 25**,** 2929-38.

MAJEED, W., MAGNUSON, M., HASENKAMP, W., SCHWARB, H., SCHUMACHER, E. H., BARSALOU, L. & KEILHOLZ, S. D. 2011. Spatiotemporal dynamics of low frequency BOLD fluctuations in rats and humans. *Neuroimage,* 54**,** 1140-50.

MALMIVUO, J., PLONSEY, R. & OXFORD SCHOLARSHIP ONLINE, N. 1995. *Bioelectromagnetism : principles and applications of bioelectric and biomagnetic fields,* New York ; Oxford, Oxford University Press.

MANTINI, D., GERITS, A., NELISSEN, K., DURAND, J. B., JOLY, O., SIMONE, L., SAWAMURA, H., WARDAK, C., ORBAN, G. A., BUCKNER, R. L. & VANDUFFEL, W. 2011. Default mode of brain function in monkeys. *J Neurosci,* 31**,** 12954-62.

MASSIMINI, M., HUBER, R., FERRARELLI, F., HILL, S. & TONONI, G. 2004. The sleep slow oscillation as a traveling wave. *J Neurosci,* 24**,** 6862-70.

MATSUI, T., MURAKAMI, T. & OHKI, K. 2016. Transient neuronal coactivations embedded in globally propagating waves underlie resting-state functional connectivity. *Proc Natl Acad Sci U S A,* 113**,** 6556-61.

MATSUURA, K. & OKABE, Y. 1995. Selective minimum-norm solution of the biomagnetic inverse problem. *IEEE Trans Biomed Eng,* 42**,** 608-15.

MESGARANI, N. & CHANG, E. F. 2012. Selective cortical representation of attended speaker in multi-talker speech perception. *Nature,* 485**,** 233-6.

NAGASAKA, Y., SHIMODA, K. & FUJII, N. 2011. Multidimensional recording (MDR) and data sharing: an ecological open research and educational platform for neuroscience. *PLoS One,* 6**,** e22561.

OGAWA, S., LEE, T. M., NAYAK, A. S. & GLYNN, P. 1990. Oxygenation-sensitive contrast in magnetic resonance image of rodent brain at high magnetic fields. *Magn Reson Med,* 14**,** 68-78.

OOSUGI, N., KITAJO, K., HASEGAWA, N., NAGASAKA, Y., OKANOYA, K. & FUJII, N. 2017. A new method for quantifying the performance of EEG blind source separation algorithms by referencing a simultaneously recorded ECoG signal. *Neural Netw,* 93**,** 1-6.

PENFIELD, W. & BOLDREY, E. 1937. Somatic motor and sensory representation in the cerebral cortex of man as studied by electrical stimulation. *Brain,* 60**,** 389-443.

POTES, C., GUNDUZ, A., BRUNNER, P. & SCHALK, G. 2012. Dynamics of electrocorticographic (ECoG) activity in human temporal and frontal cortical areas during music listening. *Neuroimage,* 61**,** 841-8.

RAUT, R. V., SNYDER, A. Z., MITRA, A., YELLIN, D., FUJII, N., MALACH, R. & RAICHLE, M. E. 2021. Global waves synchronize the brain's functional systems with fluctuating arousal. *Sci Adv,* 7.

RUBEHN, B., BOSMAN, C., OOSTENVELD, R., FRIES, P. & STIEGLITZ, T. 2009. A MEMS-based flexible multichannel ECoG-electrode array. *J Neural Eng,* 6**,** 036003.
SCHAEFER, A., KONG, R., GORDON, E. M., LAUMANN, T. O., ZUO, X. N., HOLMES, A. J., EICKHOFF, S. B. & YEO, B. T. T. 2018. Local-Global Parcellation of the Human Cerebral Cortex from Intrinsic Functional Connectivity MRI. *Cereb Cortex,* 28**,** 3095-3114.
SFORAZZINI, F., SCHWARZ, A. J., GALBUSERA, A., BIFONE, A. & GOZZI, A. 2014. Distributed BOLD and CBV-weighted resting-state networks in the mouse brain. *Neuroimage,* 87**,** 403-15.
SHARBROUGH, F. 1991. American Electroencephalographic Society guidelines for standard electrode position nomenclature. *J Clin Neurophysiol,* 8**,** 200-202.
SHOU, G., MOSCONI, M. W., WANG, J., ETHRIDGE, L. E., SWEENEY, J. A. & DING, L. 2017. Electrophysiological signatures of atypical intrinsic brain connectivity networks in autism. *J Neural Eng,* 14**,** 046010.
SHOU, G., YUAN, H., CHA, Y. H., SWEENEY, J. A. & DING, L. 2022. Age-related changes of whole-brain dynamics in spontaneous neuronal coactivations. *Sci Rep,* 12**,** 12140.
SHOU, G., YUAN, H., LI, C., CHEN, Y., CHEN, Y. & DING, L. 2020. Whole-brain electrophysiological functional connectivity dynamics in resting-state EEG. *J Neural Eng,* 17**,** 026016.
STROH, A., ADELSBERGER, H., GROH, A., RUHLMANN, C., FISCHER, S., SCHIERLOH, A., DEISSEROTH, K. & KONNERTH, A. 2013. Making waves: initiation and propagation of corticothalamic Ca2+ waves in vivo. *Neuron,* 77**,** 1136-50.
TAKAURA, K., TSUCHIYA, N. & FUJII, N. 2016. Frequency-dependent spatiotemporal profiles of visual responses recorded with subdural ECoG electrodes in awake monkeys: Differences between high- and low-frequency activity. *Neuroimage,* 124**,** 557-572.
THOMPSON, G. J., PAN, W. J., MAGNUSON, M. E., JAEGER, D. & KEILHOLZ, S. D. 2014. Quasi-periodic patterns (QPP): large-scale dynamics in resting state fMRI that correlate with local infraslow electrical activity. *Neuroimage,* 84**,** 1018-31.
TODARO, C., MARZETTI, L., VALDES SOSA, P. A., VALDES-HERNANDEZ, P. A. & PIZZELLA, V. 2019. Mapping Brain Activity with Electrocorticography: Resolution Properties and Robustness of Inverse Solutions. *Brain Topogr,* 32**,** 583-598.
UUTELA, K., HAMALAINEN, M. & SOMERSALO, E. 1999. Visualization of magnetoencephalographic data using minimum current estimates. *Neuroimage,* 10**,** 173-80.
VAN DEN BROEK, S. P., REINDERS, F., DONDERWINKEL, M. & PETERS, M. J. 1998. Volume conduction effects in EEG and MEG. *Electroencephalogr Clin Neurophysiol,* 106**,** 522-34.
VAN DEN HEUVEL, M. P. & HULSHOFF POL, H. E. 2010. Exploring the brain network: a review on resting-state fMRI functional connectivity. *Eur Neuropsychopharmacol,* 20**,** 519-34.
VAN DEN HEUVEL, M. P., MANDL, R. C., KAHN, R. S. & HULSHOFF POL, H. E. 2009. Functionally linked resting-state networks reflect the underlying structural connectivity architecture of the human brain. *Hum Brain Mapp,* 30**,** 3127-41.
VIDAURRE, D., HUNT, L. T., QUINN, A. J., HUNT, B. A. E., BROOKES, M. J., NOBRE, A. C. & WOOLRICH, M. W. 2018. Spontaneous cortical activity transiently organises into frequency specific phase-coupling networks. *Nat Commun,* 9**,** 2987.
VINCENT, J. L., PATEL, G. H., FOX, M. D., SNYDER, A. Z., BAKER, J. T., VAN ESSEN, D. C., ZEMPEL, J. M., SNYDER, L. H., CORBETTA, M. & RAICHLE, M. E. 2007. Intrinsic functional architecture in the anaesthetized monkey brain. *Nature,* 447**,** 83-6.
VIVENTI, J., KIM, D. H., VIGELAND, L., FRECHETTE, E. S., BLANCO, J. A., KIM, Y. S., AVRIN, A. E., TIRUVADI, V. R., HWANG, S. W., VANLEER, A. C., WULSIN, D. F., DAVIS, K., GELBER, C. E., PALMER, L., VAN DER SPIEGEL, J., WU, J., XIAO, J., HUANG, Y., CONTRERAS, D., ROGERS, J.

A. & LITT, B. 2011. Flexible, foldable, actively multiplexed, high-density electrode array for mapping brain activity in vivo. *Nat Neurosci,* 14**,** 1599-605.

WATROUS, A. J., FELL, J., EKSTROM, A. D. & AXMACHER, N. 2015. More than spikes: common oscillatory mechanisms for content specific neural representations during perception and memory. *Curr Opin Neurobiol,* 31**,** 33-9.

WENDEL, K., NARRA, N. G., HANNULA, M., KAUPPINEN, P. & MALMIVUO, J. 2008. The influence of CSF on EEG sensitivity distributions of multilayered head models. *IEEE Trans Biomed Eng,* 55**,** 1454-6.

YANAGAWA, T., CHAO, Z. C., HASEGAWA, N. & FUJII, N. 2013. Large-scale information flow in conscious and unconscious states: an ECoG study in monkeys. *PLoS One,* 8**,** e80845.

YUAN, H., DING, L., ZHU, M., ZOTEV, V., PHILLIPS, R. & BODURKA, J. 2016. Reconstructing Large-Scale Brain Resting-State Networks from High-Resolution EEG: Spatial and Temporal Comparisons with fMRI. *Brain Connect,* 6**,** 122-35.

ZHANG, Y., DING, L., VAN DRONGELEN, W., HECOX, K., FRIM, D. M., HE, B. 2006. A cortical potential imaging study from simultaneous extra- and intracrancial electrical recordings by means of the finite element method. *Neuroimage,* 31**,** 1513-1524.

ZHU, M., ZHANG, W., DICKENS, D. L. & DING, L. 2014. Reconstructing spatially extended brain sources via enforcing multiple transform sparseness. *Neuroimage,* 86**,** 280-93.

ZHU, M., ZHANG, W., DICKENS, D. L., KING, J. A. & DING, L. 2013. Sparse MEG source imaging for reconstructing dynamic sources of interictal spikes in partial epilepsy. *J Clin Neurophysiol,* 30**,** 313-28.